ISSN 0280-5316
ISRN LUTFD2/TFRT--5780--SE

Solving a Dead-lock Problem of NFO Sinus

Henrik Engdahl
Niklas Johansson

Department of Automatic Control
Lund University
December 2006

Department of Automatic Control
Lund Institute of Technology
Box 118
SE-221 00 Lund Sweden

Document name
MASTER THESIS

Date of issue
December 2006

Document Number
ISRNLUTFD2/TFRT--5780--SE

Author(s)
Henrik Engdahl and Niklas Johansson

Supervisor
Ragnar Jönsson at NFO Control AB in Linköping
Rolf Johansson at Automatic Control in Lund

Sponsoring organization

Title and subtitle
Solving a Dead-lock Problem of NFO Sinus (Lösning av ett baklåsproblem i NFO Sinus)

Abstract
This thesis presents, analyzes and suggests solutions to the dead-lock problem of the sensorless variable speed drive NFO Sinus. Friction, measurement, parameter estimation and quantization effects are believed possible origins of this problem and is hence studied. A short introduction to field oriented control of the asynchronous AC motor and the NFO Control strategy is also included

Keywords
sensorless motor control, asynchronous AC motor, field orientation

Classification system and/or index terms (if any)

Supplementary bibliographical information

ISSN and key title
0280-5316

ISBN

Language
English

Number of pages
73

Recipient's notes

Security classification

Acknowledgements

We would like to thank NFO Drives and especially Ragnar Jönsson for their support, for supplying us with ideas and equipment and for repairing the same after we broke it. We would also like to thank Rolf Johansson (LTH), Henrik Ohlsson (LiTH) and the staff at the Department of Automatic Control (LTH) for their help with ideas, advises on equipment and support during report writing.

Contents

Nomenclature

Symbols

ϵ	Rotor angle
ω	Rotor frequency
ζ	Stator current angle
ω_1	Stator current frequency
$\vec{i}_s/\vec{i}_r$	Stator/rotor current vector
$\vec{u}_s/\vec{u}_r$	Stator/rotor voltage vector
$\vec{i}_{mr}$	Magnetising current (rotorflux)
$L_0/L_s/L_r$	Mutual/stator/rotor inductance
R_s/R_r	Stator/rotor resistance
J	Moment of inertia
σ_s/σ_r	Stator/rotor leakage coefficients
Ψ_s/Ψ_r	Stator/rotor magnetic flux
$m_e/m_l/m_c$	Electric/Load torque/Frictional torque
u_q/u_d	Voltage vector in field coordinates
i_q/i_d	Current vector in field coordinates
u_a/u_b	Voltage vector in stator coordinates
i_a/i_b	Current vector in stator coordinates
ρ	Rotor field angle
x^q	Quantization of quantity x
p	Wordlength of digital representation

Abbreviations

ADC	Analog to digital converter
AC	Alternating Current
DAC	Digital to analog converter
NFO	Natural Field Orientation
PWM	Puse Width Modulation
VSD	Variable Speed Drive

Chapter 1

Introduction

This master thesis is written by Henrik Engdahl (LiTH) and Niklas Johansson (LTH) in cooperation with NFO Drives AB[1]. The report is published at LiTH using report number LiTH-ISY-EX–06/3945–SE and at LTH under ISRNLUTFD2/TFRT–5780–SE.

1.1 Background

Using the electrical motor to perform mechanical work is by far the most common way of utilizing electricity as a energy source [3]. Several different motor designs such as the direct current (DC) motor, the synchronous alternating current (AC) motor and the asynchronous AC motor among others is available. All motors are based on the attraction and/or repellation of two magnetic fields. What differs is the process of generating these magnetic fields. The interested reader is recommended [5] for a comprehensive survey of the most common techniques. Notation from this book will be used throughout this text and is reprinted in the beginning of this thesis. Only the asynchronous AC motor will be treated.

Figure 1.1: NFO Sinus Variable Speed Drive

NFO Drives has developed and is marketing sensorless variable speed drives in the $1.5kW$-$15kW$ range, Fig 1.1. Two patents, NFO [1] and Sinus Switch

[1] www.nfodrives.se

[2], have been filed by the inventor and company founder Ragnar Jönsson. The NFO algorithm is designed to control the rotor frequency of a asynchronous AC motor. By measuring the the controlled motors terminal voltages and currents an accurate estimation of this frequency can be made. There is no need for a tachometer mounted on the motor shaft which reduces purchase, installation and service costs.

1.2 Thesis Overview

The problem formulation as well as the models and theories important to this thesis are presented later on in this introduction. Chapter 2 describes the equipment, simulations and experiments used and Chapter 3 contains the results obtained. Chapter 4 is devoted to discussing the problem based on the observations from the preceding chapters. In Chapter 5 our conclusions and suggestions for further work can be found.

1.3 Problem Description

Problem formulation Why does the NFO algorithm fail during slow start up?

While the NFO algorithm works flawlessly after start there has been some dead-lock problems while starting the motor from zero electrical frequency. The following four symptoms are typical for the dead-lock observed:

Observation 1 While slowly increasing the speed controlling signal the motor shaft will not start rotating. Even after the control signal has increased to higher values than normal operation no rotation occurs.

Observation 2 The magnetic field is initially generated as supposed to but it increases with time in a uncontrolled manner.

Observation 3 No form of disturbance load will make put the controller into operation.

1.4 Thesis Scope

The present solution used to resolve the dead lock issue is working well in most applications but further investigation of the problem was called for. This thesis describes, analyzes and proposes design improvements (where applicable) for the following possible causes of the problem:

- *Friction* The control system does not incorporate any friction modelling or compensation. Since the dead-lock problem only arises at slow starts the Coulomb friction might have some influence.
- *Parameters* The motor parameters have to be estimated since they vary both depending on the specific motor and operating time. A faulty estimation might cause the control algorithm to act inappropriate.

- *Measurements* Currents are measured for use in the control algorithm. Errors due to inaccurate measurements will affect the performance of the regulator.
- *Quantization* All signal processing is done in a Texas Instrument TMS320C2406 DSP using fix point representation of signals and parameters [17]. The effects of the errors induced in this process might influence the performance.

This thesis is aimed for a last year student from the F-programme in Lund or the Y-programme in Linköping. The reader is assumed to be familiar with control theory, electronics, electromagnetics, mechanics and mathematics at a university level.

1.5 Asynchronous AC Motor

An asynchronous motor design does not contain expensive permanent magnets, no mechanical commutators, has low thermal and electric losses and is therefore ideal for most industrial applications. The main reason for not outperforming the alternatives completely is the lack of speed control. For a long time the DC motor was the only option due to this fact. Development of high power, low loss transistors gave rise to the electronic variable speed drive which introduces the possibility to utilize the asynchronous motor in these applications.

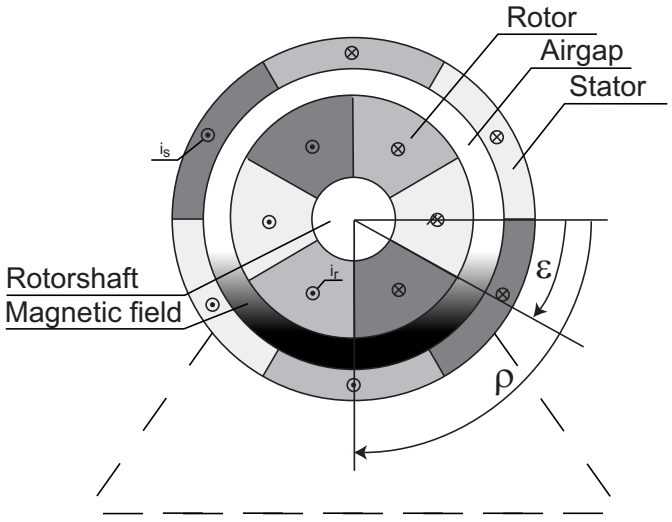

Figure 1.2: Cross section of asynchronous AC motor

The asynchronous AC motor operates by applying a rotating magnetic field onto a rotor made of a conducting material. Two different types of rotors exist, the wound and the squirrel cage. The squirrel cage motor is by far the most common and is the only one of interest in this thesis. To generate the magnetic field an electric current (i_s) flowing through the stator coils due to the applied stator voltage u_s. The rotating frequency ($\dot{\rho}$) of the magnetic field and the rotor

frequency ($\dot{\epsilon}$) do not equate when load is applied to the rotor shaft and hence its name. This motor type may also be referenced as the induction motor due to the induced rotor currents, i_r. Fig. 1.2 depicts the cross section of a general purpose AC motor.

Motor model The basic motor model has five different parameters. R_s being the resistance cause by the stator windings, R_r the resistance in the rotor, L_0 the mutual inductance between stator windings and rotor, σ_s and σ_r magnetic leakage factors for stator and rotor. The magnetic leakage may be combined into one leakage factor (σ) using Eq. (1.5) forming a four parameter model. The relationship between L_s and L_r are used for simplification and are defined by Eq. (1.6).

$$\vec{u_s}(t) = R_s\vec{i_s} + L_s\frac{d\vec{i_s}}{dt} + L_0\frac{d}{dt}(\vec{i_r}e^{j\epsilon}) \tag{1.1}$$

$$\vec{u_r}(t) = R_r\vec{i_r} + L_r\frac{d\vec{i_r}}{dt} + L_0\frac{d}{dt}(\vec{i_s}e^{-j\epsilon}) \tag{1.2}$$

$$J\frac{d\omega}{dt} = \frac{2}{3}L_0\Im[\vec{i_s}(\vec{i_r}e^{j\epsilon})^*] - m_l(t,\omega,\epsilon) \tag{1.3}$$

$$\frac{d\epsilon}{dt} = \omega \tag{1.4}$$

$$\sigma = 1 - \frac{1}{(1-\sigma_s)(1-\sigma_r)} \tag{1.5}$$

$$L_s = (1-\sigma_s)L_0 \quad , \quad L_r = (1-\sigma_r)L_0 \tag{1.6}$$

Eqs. (1.1)-(1.4) can be derived using electromagnetic and mechanical theory [5, p.154-175]. Eq. (1.1) and Eq. (1.2) describes electromagnetic interaction between stator and rotor, Eq. (1.3) the interaction between torque and the currents inside the motor and Eq. (1.4) the relationship between the rotor angle $\epsilon(t)$ and the rotor frequency $\omega(t)$. Only squirrel cage motors are considered in this thesis simplifying Eq. (1.2) since the rotor voltage $\vec{u_r} = 0$. [8, eq. 63] concludes that the asynchronous AC motor model is observable at all state values except when electrical frequency, ω_1, equals zero.

Single phase equivalent To analyse the electric properties of the AC motor a single phase equivalent circuit, also known as the inverse Γ-equivalent, is an excellent tool. This simplification is valid only if all three phases are balanced [18, p.38]. Using [5, eq. 10.66] Eq. (1.7) for stator circuit and Eq. (1.8) for rotor circuit can be derived.

$$\vec{u_s} = (R_s + j\omega_1\sigma L_s)\vec{I_s} + j\omega_1(1-\sigma)L_s\vec{I}_{mr} \tag{1.7}$$

$$0 = \frac{R_r}{\omega_{slip}}\vec{I_r} + j(1-\sigma)L_s\vec{I}_{mr} \tag{1.8}$$

$$\vec{I}_{mr} = \vec{I_r} + \vec{I_s} \tag{1.9}$$

$$\omega_{slip} = \omega_1 - \omega \tag{1.10}$$

Fig. 1.3 shows the realization of Eq. (1.7) and Eq. (1.8). Leakage inductances from both stator and rotor are contained in σL_s on the stator side of the air gap.

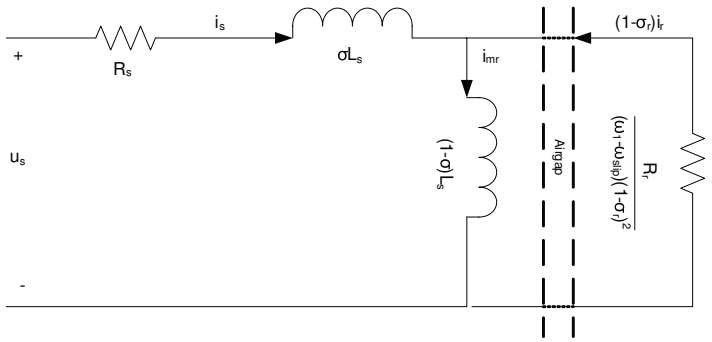

Figure 1.3: Single phase equivalent, rotor flux

The single equivalent transfer function from u_s to i_s (Eq. (1.11)) and voltage v over main inductor (Eq. (1.12)). v represents the voltage drop caused by L_s[2]. Magnetic leakage neglected.

$$\frac{I_s}{U_s} = \frac{R_R + (1-\sigma)L_s \cdot s}{R_S R_R + (R_S(1-\sigma) + R_R)L_S \cdot s + \sigma L_S^2(1-\sigma) \cdot s^2} \tag{1.11}$$

$$v = \frac{s\frac{L}{R_s}}{1 + sL\frac{R_s+R_r}{R_s R_r}} u_s \tag{1.12}$$

Field coordinates To ease the control of the AC machine an orthogonal rotating dq coordinate system, field coordinates, is used. Eq. (1.13) introduces the magnetising current[3] ($\vec{i}_{mr}$) proportional to the magnetic field ($\vec{\Psi}_r$) through the rotor [5, eq 12.22]. The vector $\vec{i}_d$ is defined to be parallel with $\vec{i}_{mr}$ and forms the angle ρ with the stator coordinates $\vec{i}_a$ vector. To create a orthogonal reference system $\vec{i}_q$ is introduced to be perpendicular to $\vec{i}_d$. See appendix A for details.

$$\Psi_R e^{j\epsilon} = L_0 \vec{i}_{mr} = L_0 i_{mr} e^{j\rho} = L_0(\vec{i}_s(t) + (1+\sigma_r)\vec{i}_r(t)e^{j\epsilon}) \tag{1.13}$$

With help of $\vec{i}_{mr}$ the unmeasurable $\vec{i}_r$ can be eliminated from Eqs. (1.1)-(1.3). By splitting the resulting equations into real and imaginary components Eqs. (1.14)-(1.18) describing the motor model in dq coordinates are formed [5, p.252-255].

$$\sigma L_s \frac{di_d}{dt} = \frac{(\sigma-1)L_s R_r}{L_r}(i_d - i_{mr}) + \sigma L_s \dot{\rho} i_q - R_s i_d + u_d \tag{1.14}$$

$$\sigma L_s \frac{di_q}{dt} = (\sigma-1)L_s \dot{\rho} i_{mr} - \sigma L_s \dot{\rho} i_d - R_s i_q + u_q \tag{1.15}$$

[2]Eq. (1.15) with constant i_{mr} and no leakage inductance

[3]Byt bas se bättre, *Arne Enqvist*

$$\frac{L_r}{R_r}\frac{di_{mr}}{dt} = i_d - i_{mr} \tag{1.16}$$

$$\dot{\epsilon} = \dot{\rho} - \omega_{slip} = \dot{\rho} - \frac{L_r}{R_r}\frac{i_q}{i_{mr}} \tag{1.17}$$

$$J\frac{d\dot{\epsilon}}{dt} = \frac{2}{3}(1-\sigma)L_s i_q i_{mr} - m_l(\omega, \epsilon, t) \tag{1.18}$$

1.6 Variable Speed Drive

The variable speed drives main functionality is to output a electric voltage at a commanded frequency. Mechanical devices have been used for this purpose but with limited areas of operation. Improvements in power electronics offer a cheap and reliable way of accurate control of the large currents necessary to operate the asynchronous motor.

Three different control approaches exist for VSD:s. The most common is open-loop control where the quotient between applied voltage and frequency is kept constant[4]. For high precision drives, a tachometer is attached to the rotor shaft making a closed-loop system possible. The third option is to measure the currents and estimate the rotor frequency. NFO is one way of achieving this estimation and controlling the inverter.

The drive consists of three parts, see Fig 1.4. The rectifier fed with line voltage producing a DC voltage, a control unit and an inverter or power amplifier to actuate the control units commands. A capacitor is used to smooth the unavoidable ripple from the rectifying process.

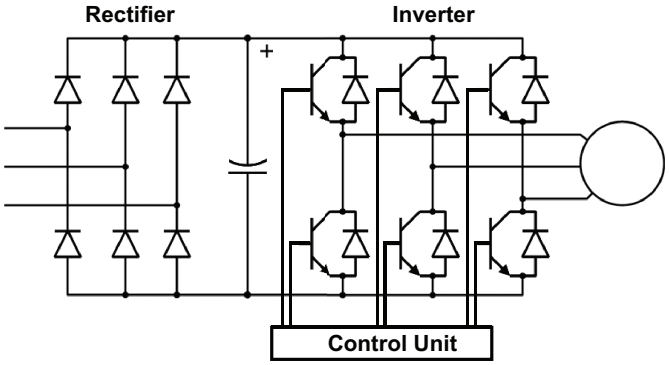

Figure 1.4: Schematics for PWM Variable Speed Drive

To minimize heat-losses in the power amplifier only on/off states are used resulting in a pulse width modulated (PWM) wave. The Sinus Switch is used for generating pure sinus voltages instead of PWM waves from the VSD. This technique is not shown in the figure and not believed to interfere with the control algorithm and will thus not be investigated further in this thesis.

[4] U/f control

Controller The NFO controller aims to invert the asynchronous motor structure in order to control it. Stator current is the only measured quantity and stator voltages serve as control signals. All control is done in field coordinates. Several other control strategies are investigated e.g. in [5] and [16].

The control strategy is to keep $|\Psi_r|$ at a constant nominal value, rotate the generated magnetic flux and compensate for slip effects due to load. Nonlinear iron properties (saturation) is the practical limitation for $|\Psi_r|$. Higher magnetic fluxes will cause the motor to operate at reduced efficiency. [4] discusses these effects briefly and provide methods for determining a correct magnetizing current. Eq. (1.14) is utilized to generate a constant i_{mr} and is considered to be efficient enough to make the approximation $di_{mr}/dt = 0$ reducing Eq. (1.17) to $i_d = i_{mr}$. Given this and neglecting magnetic leakage the governing equations for the NFO controller are:

$$u_d = R_s i_{mr} \tag{1.19}$$

$$\rho = \int_0^t \dot{\rho} dt \tag{1.20}$$

$$\dot{\epsilon} = \dot{\rho} - \omega_{slip} \tag{1.21}$$

$$\dot{\rho} = \frac{u_q - R_s i_q}{L_s i_{mr}} \tag{1.22}$$

$$\omega_{slip} = \frac{R_r i_q}{L_r i_{mr}} \tag{1.23}$$

1.7 Friction

The AC motor model in Eqs. (1.1)-(1.4) does not consider friction. The classical Coulomb/Viscous friction, the Dahl model [6] and the LuGre model [7] are three possibilities to capture this phenomenon. Dahl's friction model for rotating bodies is described by Eq. (1.24)[5] where m_c is the Coulomb torque and σ_f a stiffness constant [9, p.10]

$$\frac{dm}{dt} = \sigma_f \omega \left(1 - \frac{m}{m_c} sgn(\omega)\right) \tag{1.24}$$

1.8 Parameter Sensitivity

Successful control of the motor requires accurate knowledge of the parameters in Eqs. (1.19)-(1.23). General parameter estimation schemes such as described in [12] uses PRBS to excite all possible states. This is not necessary for the electric motor thanks to the detailed knowledge of the system where only a small subset of states has to be exited. By applying signals of nominal amplitude at one phase at a time amplitude the identification process can be performed with no disturbances in rotor angle which means the single phase equivalent may be used as a complete model of the system. Examples of estimation techniques are found in 2.4.

[5] Derived in Appendix F

1.9 Measurements

No sensors are perfect. To describe the measurement imperfections the simple model described in Eq. (1.25) where $s(t)$ is the measurement, $e(t)$ white noise and a an offset can capture the characteristics of the current measurement.

$$y(t) = s(t) + e(t) + a \tag{1.25}$$

SNR is calculated with equation Eq. (1.26) where P denotes effect and A amplitude.

$$SNR = \frac{P_{signal}}{P_{noise}} = \left(\frac{A_{signal}}{A_{noise}}\right)^2 \tag{1.26}$$

1.10 Quantization

Quantization effect will occur due to the digital implementation of the controller. Measured signals, output signals and internal calculations will be performed with a precision limited by the DSP:s word length.

To make good use of the number of available bits, p, the maximum signal value, x_{max}, should generate the highest representable value digital value, $d_p = 2^p$. To achieve this scaling coefficients, K_x, are used for both signals and constants according to Eq. (1.27) and Eq. (1.28). The smallest representable difference between two values is calculated with Eq. (1.29). Note that the scaling of measured signals usually is done with analog circuits to utilize the full potential of the analog to digital converter (ADC).

$$K_x = \lfloor \frac{d_p}{x_{max}} \rfloor \tag{1.27}$$

$$x^q = K_x x_{measured/constant} \tag{1.28}$$

$$x^q_{min} = \lceil \frac{1}{K_x} \rceil \tag{1.29}$$

The method for calculating K_x is essentially the same as when working with the Per Unit (P.U) system [18, p. 96-103]. Derived constants, K_r e.g., can be treated as derived P.U. quantities .

The quantization effect will cause changes in signals always to occur as step changes with minimum step size of x^q_{min}. A continuous ramp, $y = kx$, will be approximated with a series of steps, a staircase function. The step size is dependent on T_s and k. If k and T_s is small the changes in x shrinks to x^q_{min}.

The characteristics of the quantization disturbance $e_q(t) = x(t) - x^q(t)$ is dependent on the quantization technique. A correctly rounded value will have $E(e_q) = 0$ and no correlation between samples. Using a floor and ceiling function causes $E(e_q) \neq 0$ which essentially is an offset error.

The SNR for a high resolution AD converter can according to [20] be approximated to :

$$SNR_{ADC} \approx 6p[dB] \tag{1.30}$$

Chapter 2

Materials and Methods

Every section in the preceding chapter has been investigated analytically as far as possible. For confirmation of the results simulations and experiments presented in this chapter have been used. Effects like rounding have only been studied in simulations due to the nonlinearities of the system.

All reference equipment was kindly provided by NFO Drives AB and the Department of Automatic Control at LTH. The differences between the production drive and our test equipment are listed in Tbl. B.4. Results of the analysis, simulations and experiments can be found in Chapter 3.

To avoid unnecessary exposure of source code and to reduce the differences between simulation and experiments the VSD was connected directly to Simulink using LTH:s I/O-card[1], Fig. 2.1.

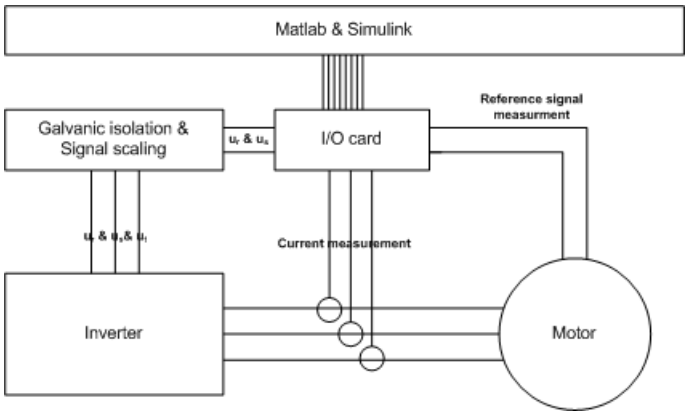

Figure 2.1: Experiment setup overview

Since no real time operating system is available the highest possible sampling rate is about $1kHz$. At higher sampling rates too many deadlines are missed to control the motor correctly. To reduce the interference from the window manager remote control of the computer via secure shell (SSH) was used. To

[1]No specification of the card was to be found. For questions we refer to Rolf Braun at Department of Automatic Control, LTH

protect the power electronics voltage and current limitations (red blocks) were introduced[2] into the motor control block in Fig. 2. This block also provides the bootstrap sequence described in Appendix B as well as offset compensation and scaling for both control voltage and measured quantities. No measurements are made and no control signals was forwarded to output before the necessary bootstrap sequence was completed.

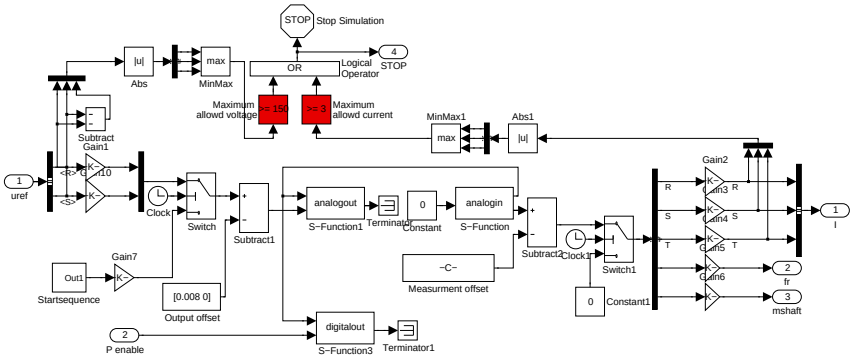

Figure 2.2: Simulink motor control block

Some hardware modification was required to control the inverter from Simulink with LTH:s I/O-card. Most important was to provide galvanic isolation between the computer and the circuits of the VSD. The isolation amplifier ISO124 provides this service. The input of the work point for the ADC on the VSD is $2.5V$ with a swing of $2.5V$. The equipment provided by LTH outputs voltages in the range $\pm 10V$ with two DAC:s. One OP07 from Analog Devices and three TLC2274ACH from Texas Instrument together with precision resistors does this conversion. Two trimming potentiometers were used for offset compensation between the phases. All this was constructed and wire-wrapped by Ragnar Jönsson who also helped us to trim the system. To ensure the correct signal is fed to the power amplifier a series of measurements was made. The results are listed in Tbl. B.3 and the circuit schematics in Appendix E.

2.1 Asynchronous AC Motors

Two standard 3-phase, $1.5kW$, Y-connected asynchronous motors have been at our disposal during the project. Motor data is listed in Tbl. B.1. Both motors are equipped with flywheels to increase the moment of inertia and provide the possibility to apply external torque. Measured parameters were acquired according to protocols specified in 2.4.

Models Two different motor model implementations were used for simulation purposes. One provided by NFO Drives developed with in dq coordinates and based on Eqs. (1.19)-(1.23) and one provided by Mathworks through the Simulink SimPower toolbox [19]. Both originate from the same basic equations

[2] After the first breakdown

(Eqs. (1.1)-(1.4)) and should therefore behave in the same way. The purpose of using two different models is to reduce the possibility of having erroneous implementations.

Validation experiment To confirm that the models are interchangeable the difference (Δf, Δm_e) of the output when applying the same stimuli variables was calculated.

2.2 Variable Speed Drive

NFO Drives supplied a modified NFO Sinus $1.5kW$ inverter equipped with the Sinus Switch for test purposes. In the unit provided the controller card connections to the DSP and DAC had been removed and wires soldered for connection to a wire-wrap plate. Tbl. B.2 lists which wire color that corresponds to which signal.

Controller implementations The power electronics dynamic behavior are assumed to be fast in comparison to the demands issued by the controller[3]. Four versions of the controller have been implemented in Simulink for simulation and control via the I/O-card:

1. NFO Drives implementation used as reference while constructing our continuous-time model.

2. Continuous-time model of the controller based on Eqs. (1.19)-(1.23), u_q as control signal.

3. Continuous-time model as above with Eq. (2.1) and Eq. (2.2) for current and speed control.

4. Discrete sampled controller for simulating the effects of the DSP implementation with u_q as control signal.

$$u_{q_{ref}} = K_{pi}(i_q - i_{q_{ref}}) + K_{ii}\int_0^t i_q - i_{q_{ref}}dt \tag{2.1}$$

$$i_{q_{ref}} = K_{p\omega}(\hat{\omega} - \omega_{ref}) + K_{i\omega}\int_0^t \hat{\omega} - \omega_{ref}dt \tag{2.2}$$

Validation experiment To confirm the suggested improvements the control algorithm of a second NFO Sinus unit was modified. Ramping the speed reference from $0Hz$ to $1Hz$ during different time periods is possible with the user interface. By changing the time period a quantitative measurement of modifications impact can be obtained. Ten consecutive starts without dead-lock is regarded as a successful test. The modifications were performed by Henrik Hemark, NFO Drives.

[3]Kenneth Svensson, *NFO Drives*

2.3 Friction

Estimation of m_c The maximum frictional torque, m_c, is required in all friction models. The experiment is based on Newton's second law for rotating bodies:

$$J\frac{d\omega}{dt} = m_e - m_l \tag{2.3}$$

At constant ω, m_e equals m_l. When unplugging the power source the electric torque m_e is removed and the load torque will stop the rotation. Then by measuring the frequency $d\omega/dt$ can be estimated. J is given by the motors data sheet making the calculation of m_l trivial. Some attention should be paid to the initial decrease in rotational speed. The magnetic fields inside the motor when the power source is disconnected will initially have a braking effect on the rotor. Hence m_l is not only frictional torque. The electromagnetic effects will decay quickly giving a measurement of m_c. This test is a reduced version of [14, p.280-281].

High friction Since the normal friction of the motor a small the friction effects is hard to investigate. Locking the rotor will have the same effect as an extremely high static friction. This experiment may be used to investigate the validity of Eq. (3.1).

2.4 Parameters

Parameter estimation By investigating the frequency response of the motor, in simulation, it is possible to find at what frequencies what parameters should be calculated. The bode plots of the single phase equivalent, described by Eq. (1.11), with different parameters are shown in fig. 3.7.

There are many ways to retrieve the electric parameters of the single phase equivalent. In the NFO sinus there is sophisticated algorithm to derive the parameters but the following scheme may be used to get a rough estimate. Keep the top bode plot in fig. 3.7 and the following equations in mind (derived from Eq. (1.11)):

$$\frac{\partial}{\partial s}\frac{I_s}{U_s} = \frac{1}{\frac{R_S(1-\sigma)+R_R}{(1-\sigma)} + 2\sigma L_S \cdot s} \tag{2.4}$$

$$\frac{\partial}{\partial s}\frac{I_s}{U_s} \to \frac{1}{2\sigma L_S}, \quad s \to \infty \tag{2.5}$$

R_s Apply small DC voltage and measure the current flowing through the winding. Use Ohm's law to calculate R_s. Remember to compensate for Y and Δ connected motors. Also bear in mind that it takes some time for the motor to stabilize, sometimes minutes for big motors. This method may be used since Eq. (1.11) equals $\frac{1}{R_s}$ when $\omega(= s) = 0$.

σ Run the motor at rated speed. Measure the voltage U and current I. The phase difference ϕ between U and I is related to σ as $cos(\phi) = (1-\sigma)/(1+\sigma)$ [5, eq 10.75]

L_s Using Eq. (2.5) and knowing σ, L_s may be derived measuring the derivative at a high frequency.

R_r Apply a small sinusoidal voltage U with a frequency around 50 Hz (somewhere in the middle or the bode plot in fig. 3.7). At this terrace, before the steep slope, the following equation holds $\frac{I}{U} = \frac{1}{R_s+0.5R_R}$. intuitively the factor 0.5 comes from half the current going through the rotor resistor and half the current through the main inductor.

Parameter sensitivity The aim is to find a range in which R_s, L_s, R_r and σ may lie and still have a working controller that gives an acceptable behavior. Compare run sequences with one of the parameters askew to a test sequence with proper parameters. Determine how much error there may be in the parameters and still have the motor to behave nicely, close to the run with correct parameters.

2.5 Measurements

Current measurement To simplify the experimental setup the current transducers used in production was not used while conducting experiments. Three LEM-Module 300-S wound 30 times were used for this purpose. Most of the offset induced by the power amplifier was compensated for using the trimming potentiometers and the fine-tuning was done in software.

Sampling the output of the LEM-modules and analysing the covariance and the signal spectrum of the result verified the model. The signal is defined to be the amplitude of the smallest current flowing through the motor. Using the NFO controller this will be the magnetizing current.

Speed and torque measurement For reference purposes a tachometer with a resolution of $4000 pulses/turn$ and a tension torque measurement unit with a range of $\pm 30 Nm$ were available. Only torque at standstill may be measured. The sampling rate is the same as for the whole system.

2.6 Quantization

The quantization phenomena were investigated using simulations of the discrete controller. This controller makes it possible to easily manipulate the level of quantization and rounding techniques in a way not possible in the real controller.

Chapter 3

Results

All experiments were conducted with equipment described in Chapter 2. Measured speed and torque signals were low pass filtered to suppress noise due to quantization (Appendix C.2). Input signals were specified as $nx2$-matrices, see example of $H(t)$ in table 3. Values between specified points were linearly interpolated.

t	-1	0	0	1
v	0	0	1	1

Table 3.1: $H(t)$

3.1 Asynchronous AC motor

Dead-lock conditions Using Eqs. (1.13) and Eq. (1.18) condition 1-3 for avoiding dead-lock was found. These conditions will be used to examine the possible dead-lock causes.

Condition 1 A magnetic field has to be generated implying $i_{mr} > 0$

Condition 2 If condition 1 is fulfilled Eq. (1.18) concludes that $i_q \neq 0$ in order to create any torque and thereby angular acceleration $(d\omega/dt)$ for the rotor.

Condition 3 The magnetic field must rotate, $\rho(t) \neq \rho(t - \Delta t)$.

Validation experiment Simulated values for Δm_e and Δf for the two motor models when fed with $10Hz$ $15V$ three phase voltage. With a locked rotor shaft, the difference in generated torque was identical to Fig. 3.1. Except for the obvious oscillative difference an offset in Δm_e were noted. This offset causes the increasing error in Δf. Both errors are small compared to normal operating conditions.

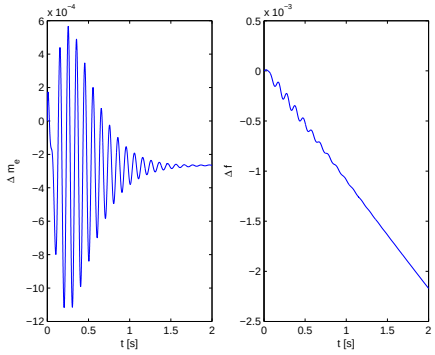

Figure 3.1: Difference of motor models output

Using a more complex control signal more of the motors states can be excited. For these simulations the continuous NFO controller was used, see Fig. 3.2. The overshoots can be reduced by increasing the gain of the speed PI controller. Deviations up to 15% between the models are observed at step changes in reference speed. The NFO motor model always was closest to the reference signal.

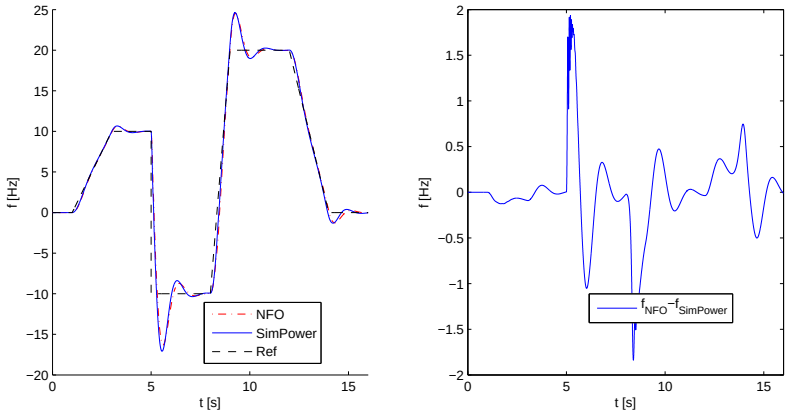

t	0	1	3	5	5	8	9	12	14
f_{ref}	0	0	10	10	-10	-10	20	20	0

Figure 3.2: Simulation of controlled motor models and difference in rotor frequency

To compare the models to a real motor the same control sequence was fed to our test rig. The results in Fig. 3.3 are not completely comparable since the the discrete-time sampled controller has been used. The exact parameters of the motor are also unknown which affects the results. The error between 1 and 3 s may be due to lack of friction compensation. Erroneous parameters and friction may cause the offset error at 6-8 s and 10-12 s.

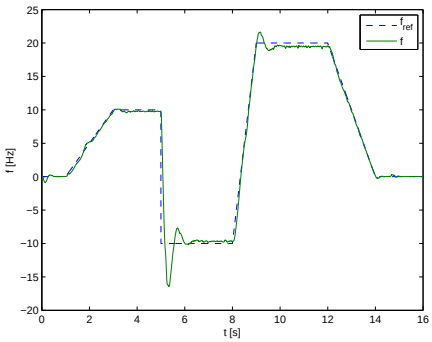

t	0	1	3	5	5	8	9	12	14
f_{ref}	0	0	10	10	-10	-10	20	20	0

Figure 3.3: Rotor speed control test

The Matlab `step`-function was used for calculating step response for Eq. (1.11) and Eq. (1.12). The maximum voltage over the main inductor was almost the same even if the motor size increases with a factor 20 as seen to the left in Fig. 3.4. Initial current values differ with several orders of magnitude as seen to the right in the same figure.

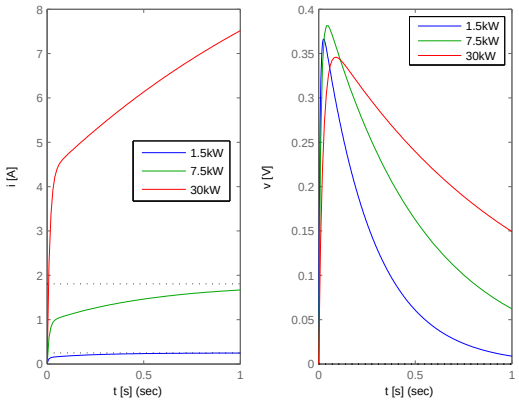

t	0	0	1
u_q	0	1	1

Figure 3.4: Single phase equivalent step response for different sized AC motors

3.2 Variable Speed Drive

Validation experiment The result in Tbl. 3.2 was retrieved after modifying the hardware according to improvements suggested in the discussion. Unsuccessful tests is marked with a − in the following table.

Modification	Minimal ramp for successful test Hz/s
No modification	1
Reduction of PI sample rate: 800Hz	0.25
Reduction of PI sample rate: 400Hz	-
Pre-quantization of u_q to $u^q_{q_{min}} = 3.2V$	0.25
Pre-quantization of u_q to $u^q_{q_{min}} = 6.4V$	0.1

Table 3.2: Tests with NFO Sinus unit

3.3 Friction

Condition 2 is derived from Eq. (1.18) where m_l is a general load torque, with friction included. The frictional forces are small but with their constant presence makes them a candidate to causing the dead-lock. At low torques, e.g. initially at slow starts, m_c is higher than m_e. The hypothesis is that friction puts the regulator out of play if not conquered quickly.

Eq. (3.1) is Eq. (1.15) and Eq. (1.18) combined. At standstill $\dot{\rho} \approx 0$, with typical values for $\sigma L_s < 0.05$ and i_{mr} controlled by u_d the torque is in essence controlled by u_q.

$$m_e = \frac{2}{3}(1-\sigma)\frac{L_s}{R_s}\left(u_q - \sigma L_s \dot{\rho} i_d - (1-\sigma)L_s \dot{\rho} i_{mr} - \sigma L_s \frac{di_q}{dt}\right) i_{mr} \qquad (3.1)$$

Observation 2 indicates that the i_{mr} control is successful. The motor is supposed to generate torque even at standstill if $u_q \neq 0$. Fig. 3.6 verifies this. If the commanded u_q is large enough to generate a torque larger than m_c the shaft should start to rotate.

Coulomb/Viscous friction This classical friction model was abandoned quickly due to its discontinuity causing the simulation to hang. A discussion of the problem and a solution, the Karnopp Model, can be found in [9, p.9]. This suggestion was not of interest to us since it does not simulate stiction.

Dahl´s friction model The model was implemented and worked well during simulation.

LuGre friction model The LuGre friction model was implemented, sparsely tested but was discarded due to its many parameters. The σ_f value from [7] was used in all simulations.

Estimation of m_c m_c estimated to 0.44 Nm by using the average $d\omega/dt$ from measurements calculated with the script found in C.1. Figure 3.5 plots the measured and simulated data. The initial breaking effect of the magnetic field is clearly affecting the rotor speed in the simulations. This is not as obvious for the measured data.

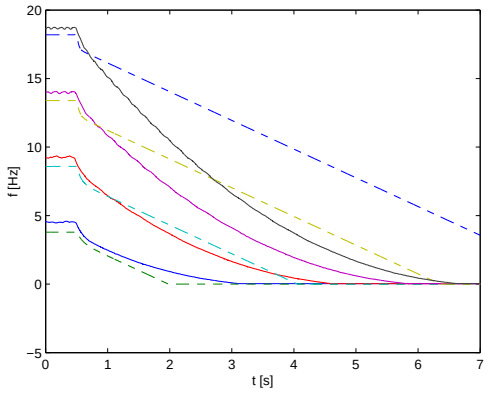

Figure 3.5: Simulation and experimental results for friction estimate

High friction For the investigation of the impact of high friction this experiment was carried out. The discrete sampled controller without the speed and current PI controllers was used. Ramping the control signal u_q should according to Eq. (3.1) generate a proportional torque. Fig. 3.6 proves that this was a correct assumption for our system. If the rotor was manually turned backwards and released the rotor started to rotate as supposed to. No dead-lock occurred.

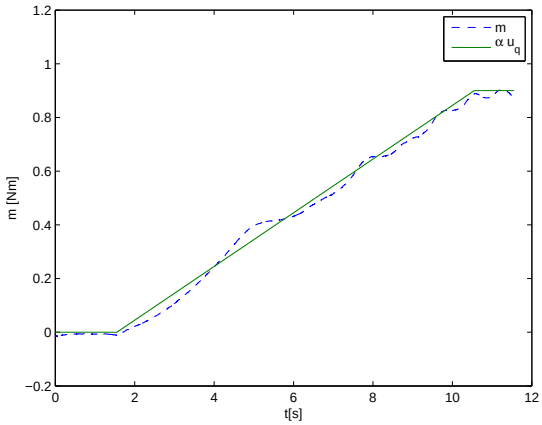

Figure 3.6: Torque generation with locked rotor

3.4 Parameters

Parameter estimation Fig. 3.7 Bode plot (upper figure) for the single phase equivalent and simulation results (lower figure) for the whole system while varying R_s. Differences for both amplitude and phase may be noted. Plots where R_r and L_s is modified can be found in Appendix D.3.

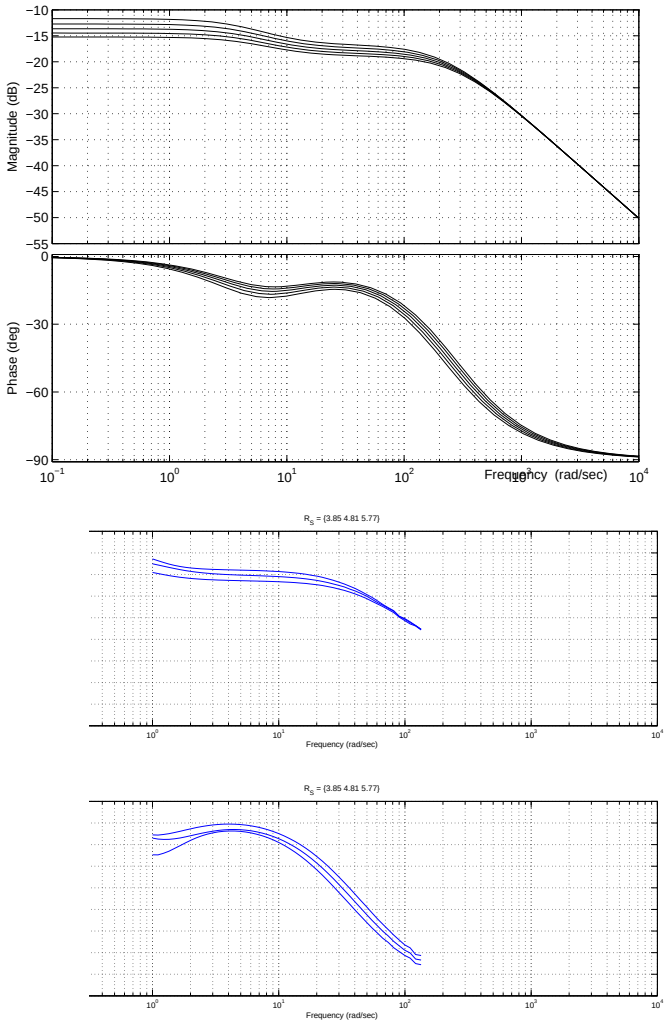

Figure 3.7: Bode plot and simulation results for different values of R_s

The "norm". Test sequence ran using the correct parameters.

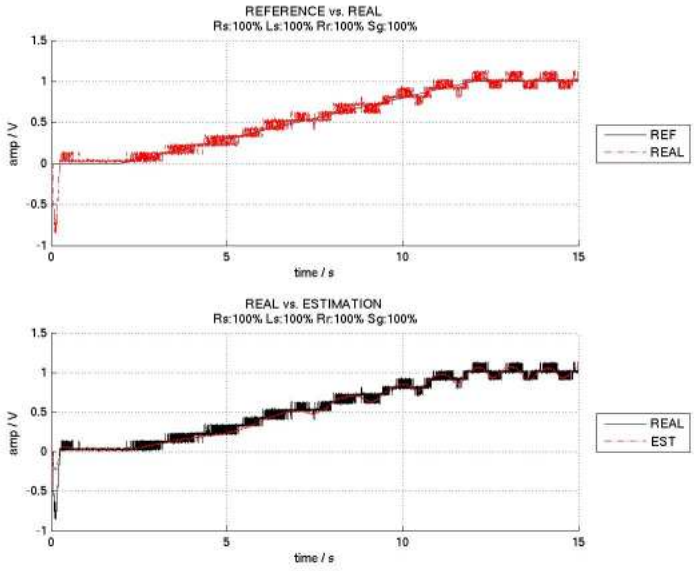

Figure 3.8: Test sequence with correct parameters

R_S only 30% of correct value but still acceptable behavior.

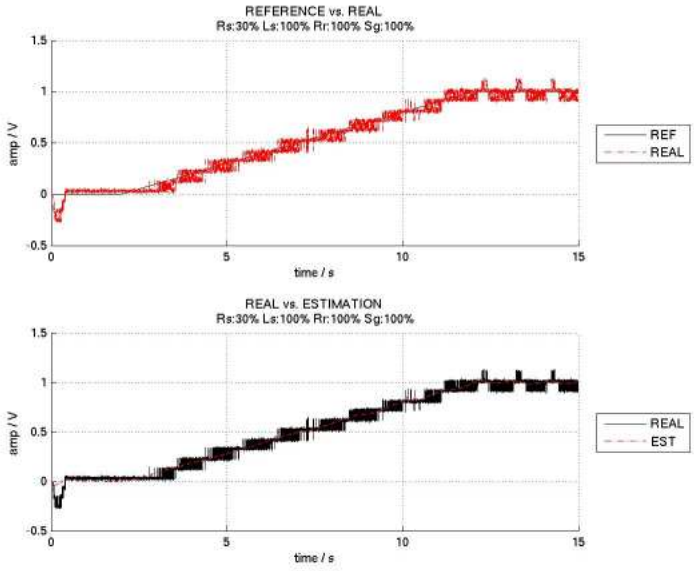

Figure 3.9: R_s at 30%

The upper bound of R_S. Correct behavior.

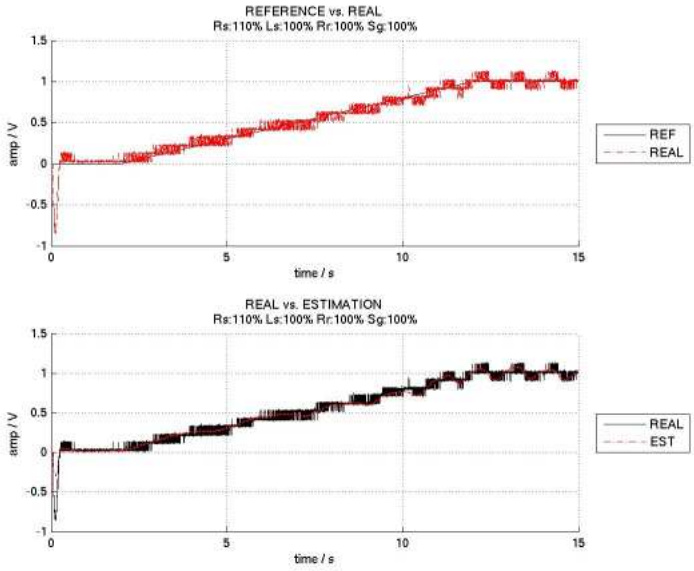

Figure 3.10: R_s at 110%

Unacceptable behavior. R_S over estimated.

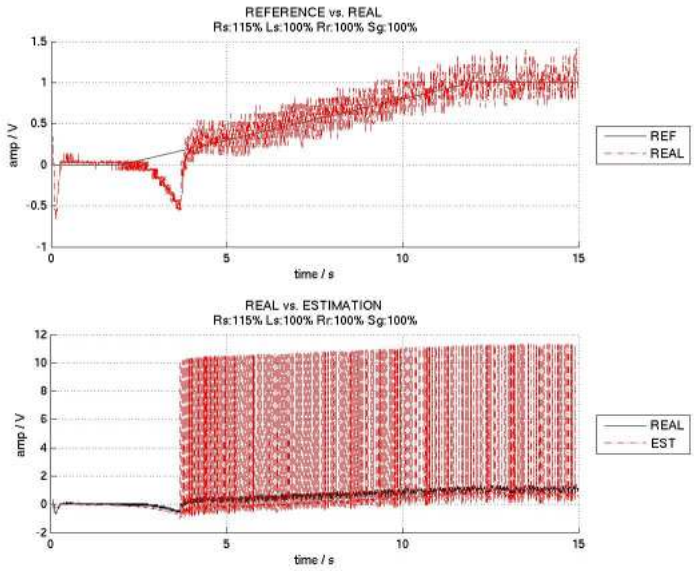

Figure 3.11: R_s at 115%

Compared to the "normal" figure this behavior is not good but acceptable.

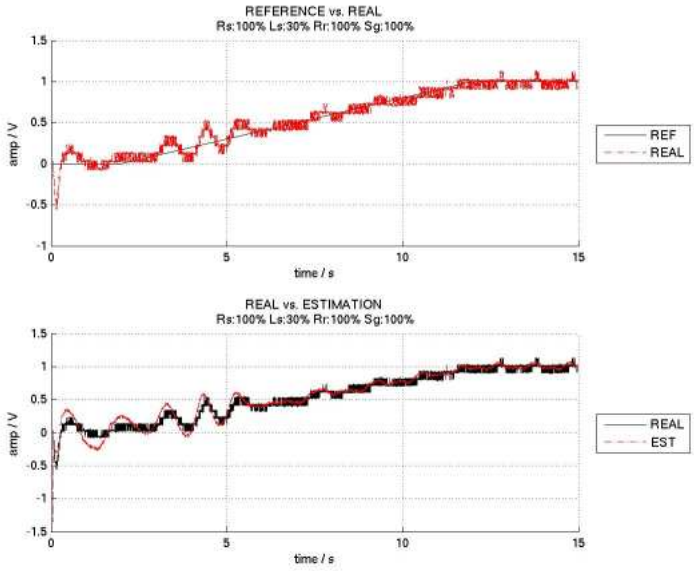

Figure 3.12: L_s at 30%

The lower bound of estimation of L_S.

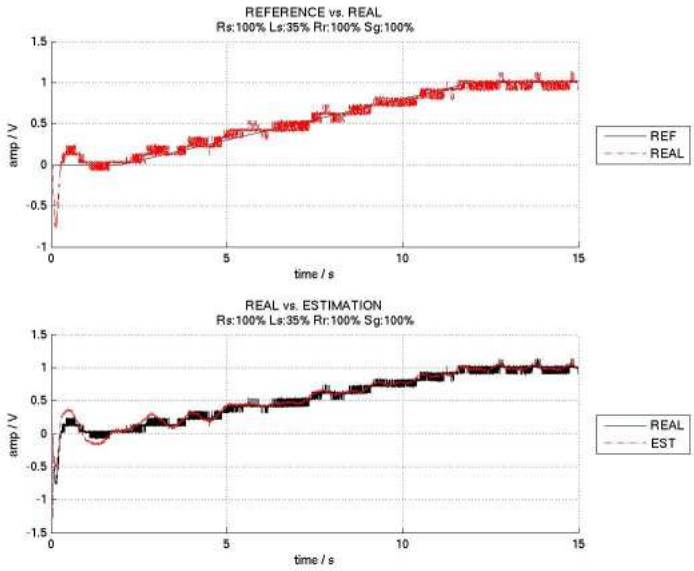

Figure 3.13: L_s at 35%

The upper bound of estimation of L_S.

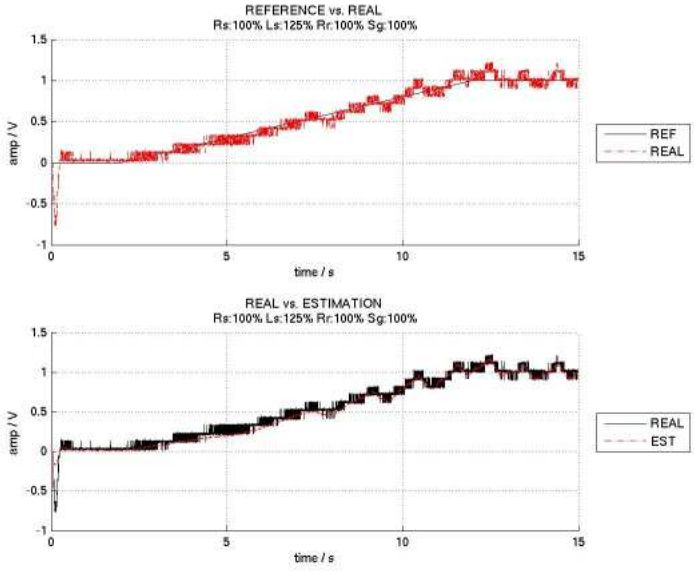

Figure 3.14: L_s at 125%

Overestimation of L_S. Note the same size "spikes" in estimation (bottom).

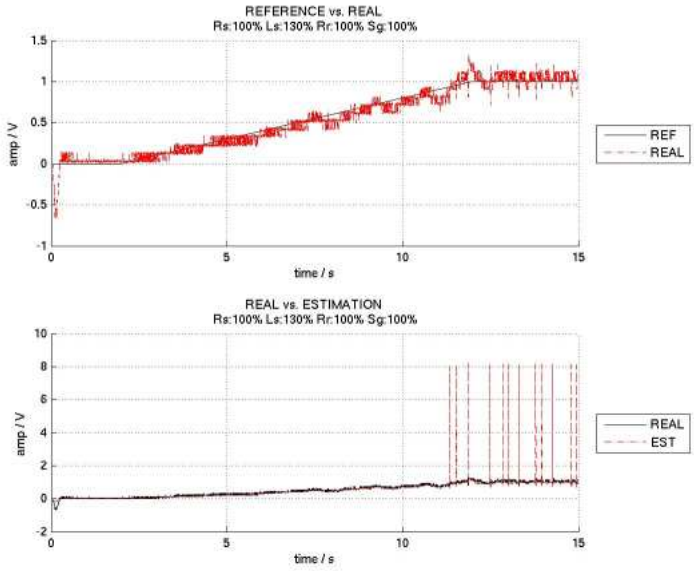

Figure 3.15: L_s at 130%

The smallest R_R that was tested. Still good behavior.

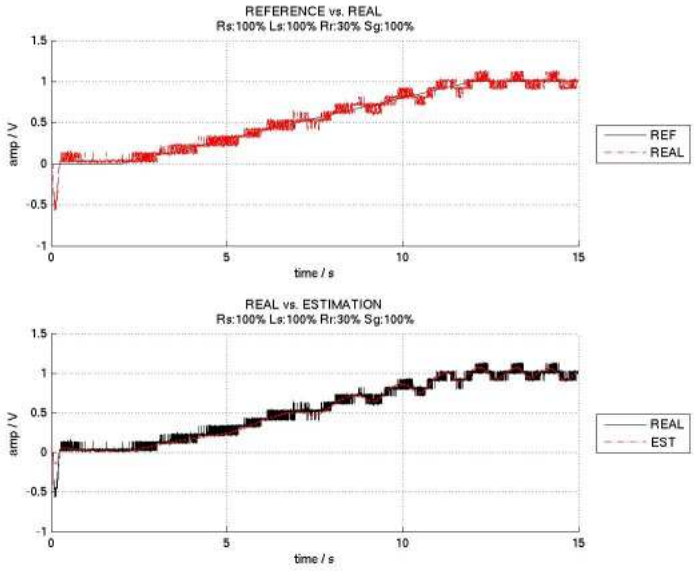

Figure 3.16: R_R at 30%

The largest R_R that was tested. Still good behavior.

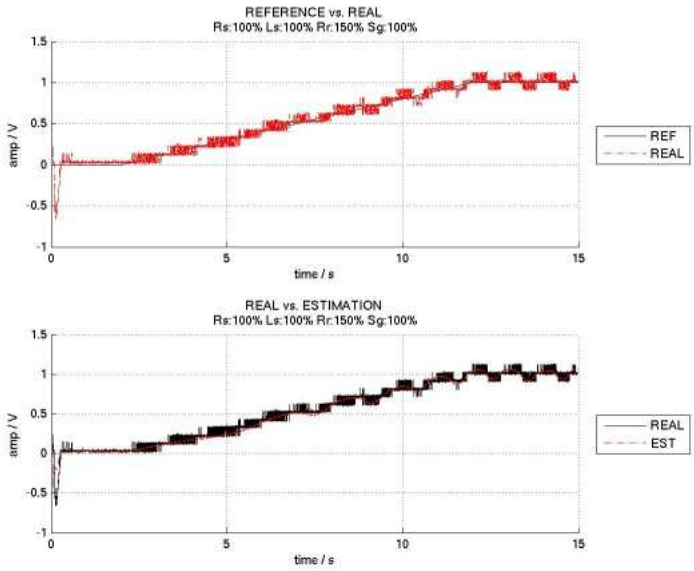

Figure 3.17: R_R at 150%

The smallest σ that was tested. Still good behavior.

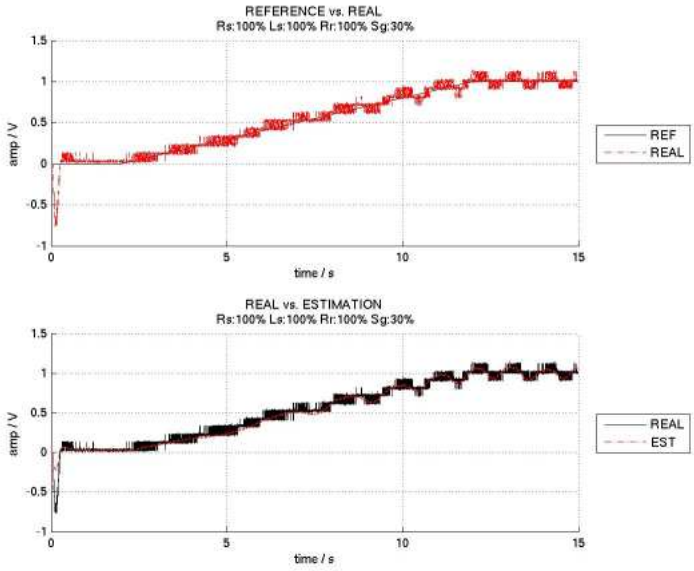

Figure 3.18: Sigma at 30%

The largest σ that was tested. Still good behavior.

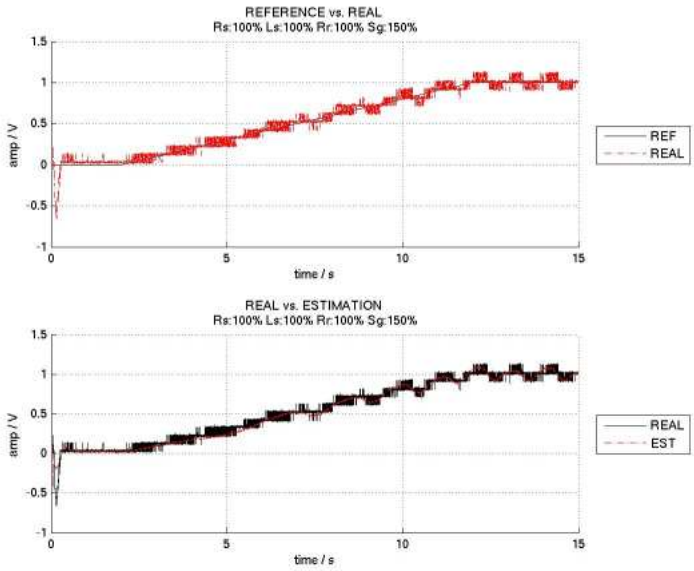

Figure 3.19: Sigma at 150%

Mixed test sequence Underestimation of R_S.

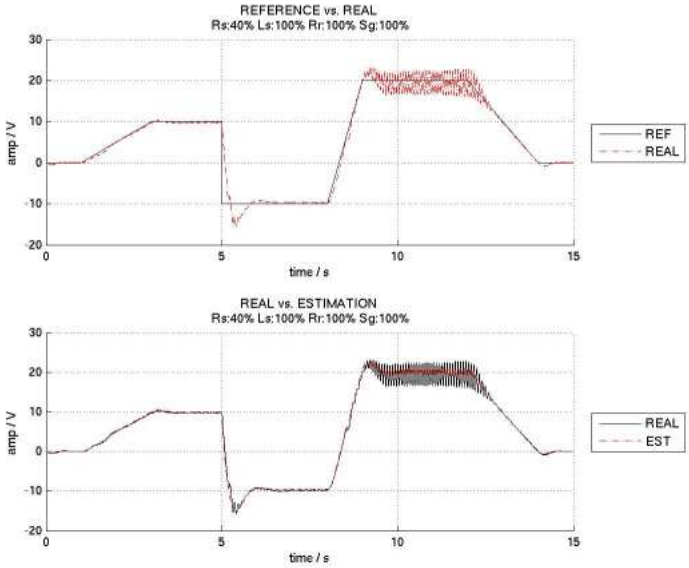

Figure 3.20: R_s at 40%

Acceptable behavior, lower bound R_S.

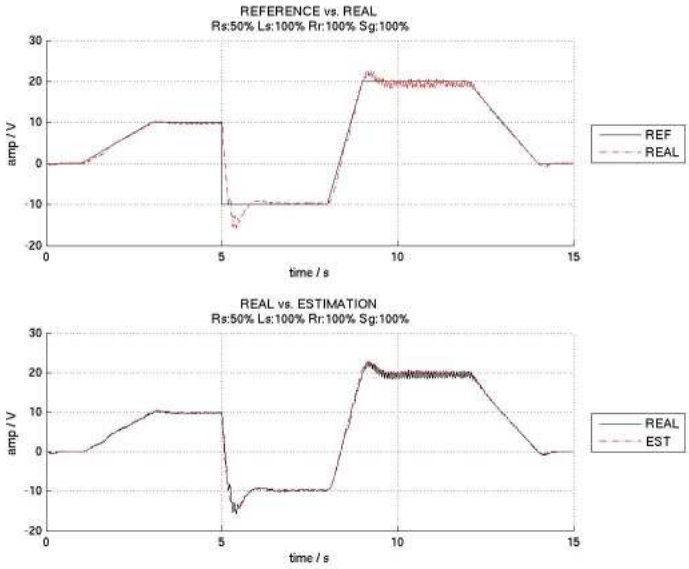

Figure 3.21: R_s at 50%

Upper bound R_S.

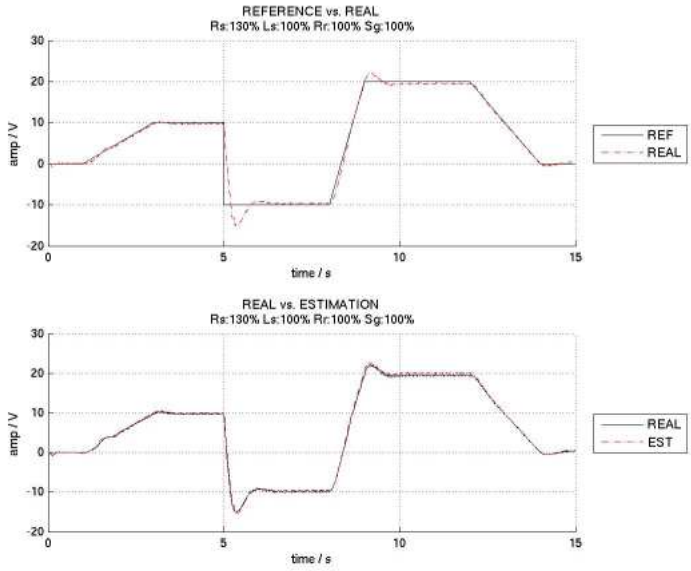

Figure 3.22: R_s at 130%

Test sequence not finished due to extreme currents. Overestimated.

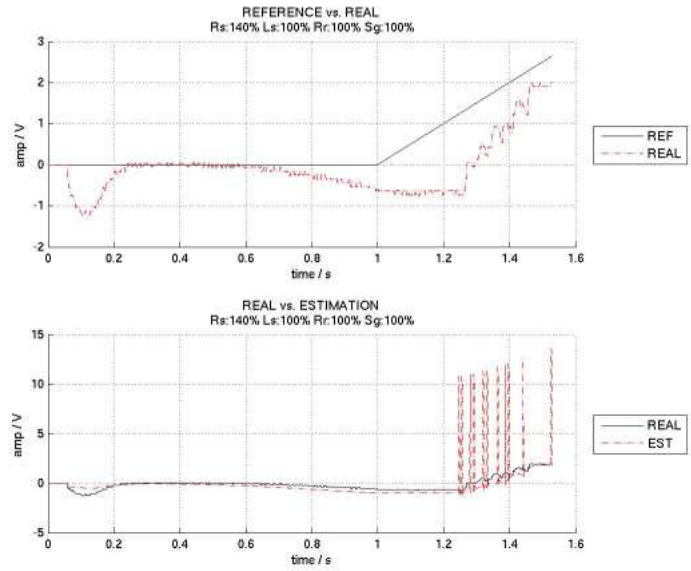

Figure 3.23: R_s at 140%

Smallest L_S that was tested, good behavior.

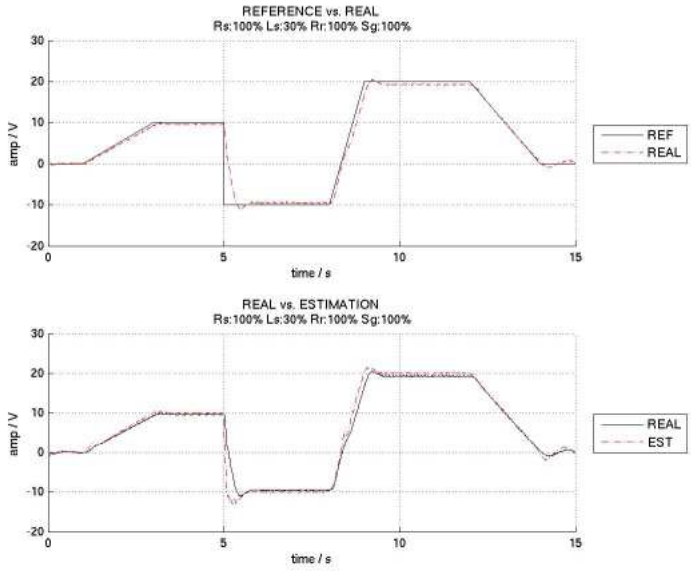

Figure 3.24: L_s at 30%

Upper bound L_S.

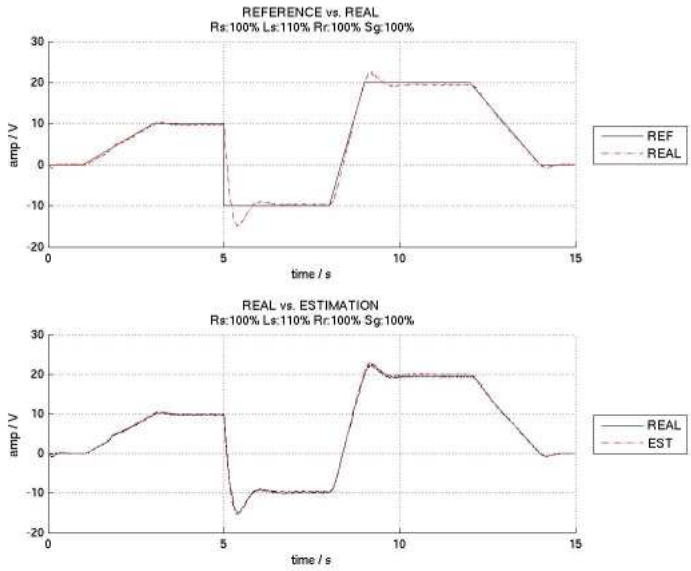

Figure 3.25: L_s at 110%

Test sequence not finished due to extreme currents. Overestimated L_S

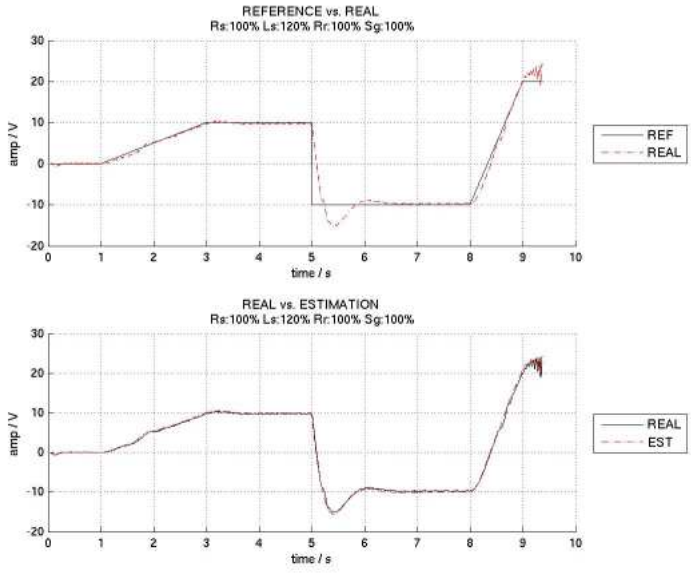

Figure 3.26: L_s at 120%

Smallest σ being tested. Acceptable behavior.

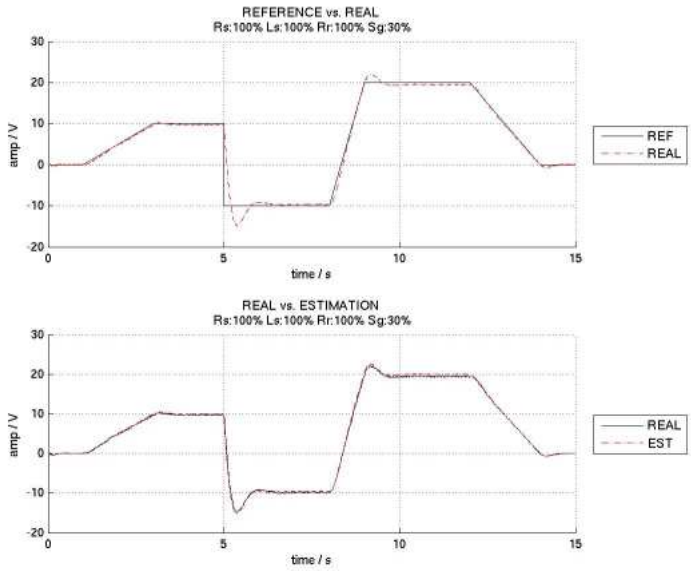

Figure 3.27: Sigma at 30%

Upper bound of σ. Also norm for test sequence, since all parameters are at their correct values.

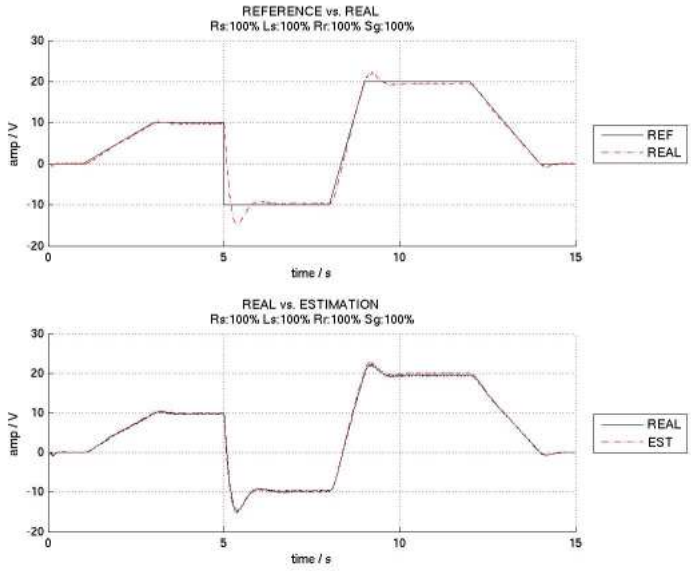

Figure 3.28: Normal, incl Sigma at 100%

Test sequence did not finish due to extreme currents. Overestimated σ.

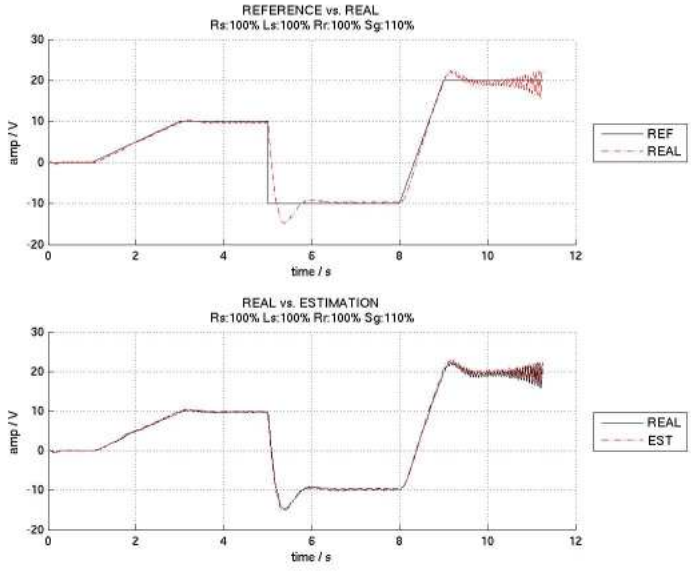

Figure 3.29: Sigma at 110%

3.5 Measurements

The test equipments SNR is about 80 dB.

To make ordinary error propagation analysis beyond the conversion to the ab coordinate system is not possible due to the mutual dependence between ρ and i_q:

$$\begin{aligned} i_q &= \cos(\rho i_b) - \sin(\rho i_a) \\ \rho &= \int_0^t \frac{u_q - R_s i_q}{L_s i_{mr}} dt + \sigma \frac{i_q}{i_{mr}} \end{aligned}$$

Current measurement Any disturbances effecting the three phases equally will be suppressed by using the first transformation matrix of Eq. (A.2). If n_r, n_s and n_t are similar signals they will cancel in Eq. (3.2) but if Eq. (3.3) is used the disturbance n_r will be enhanced by a factor 3/2. i_b is unaffected by the choice of transformation.

$$i_a = (i_r + n_r) - \frac{1}{2}(i_s + n_s) - \frac{1}{2}(i_t + n_t) \tag{3.2}$$

$$i_b = \frac{3}{2}(i_r + n_r) \tag{3.3}$$

The FFT of the measured data was as constant except for the small deviation in low frequencies, Fig. 3.5. By turning off the power electronics of the VSD their impact on the current measurement could be investigated, Tbl 3.5.

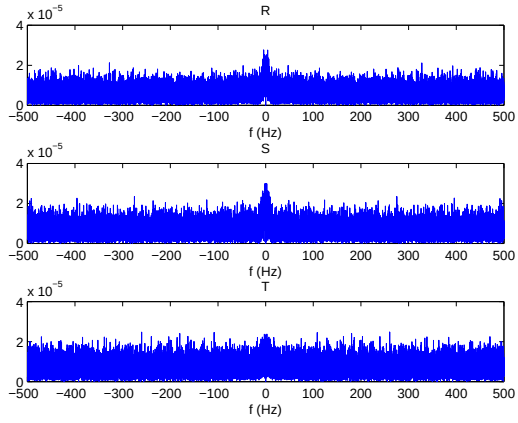

Figure 3.30: FFT of measurement noise from LEM-modules

	Power Enabled			Power Disabled		
	R	S	T	R	S	T
Mean	0.0062	0.0083	-0.0055	0.0041	0.0084	-0.0049
Cov.	3.959e-5	7.108e-5	3.234e-5	1.781e-5	7.155e-5	2.499e-5
Max	0.0188	0.0165	0.0119	0.0085	0.0142	0.0105

Table 3.3: Noise properties at current transducers

3.6 Quantization

Condition 1 is marginally affected by quantization. $R_s i_{mr}$ is constant and $\dot{\rho} \approx 0$ in Eq. (1.19) at low speeds. Commanding $u_d > u^q_{d_{min}}$ causing $i_{mr} > 0$ which satisfy condition 1. Eq. (1.15) implies condition 2 is also met since $i_q \neq 0$ if $u_q > u^q_{q_{min}}$.

To analyse condition 3 Eq. (1.20) and Eq. (1.21) has to be considered. The integration is approximated with the sum $\rho^q = \sum_0^{nT_s} T_s \dot{\rho}^q$ implemented using forward Euler giving the condition $1 < \lfloor |T_s \dot{\rho}^q| \rfloor$ to change its value. $\dot{\rho}$ is generated from Eq. (1.22) yielding inequality 3.4.

$$1 < \lfloor \left| \frac{T_s}{L^q_s i^q_{mr}} v^q \right| \rfloor \tag{3.4}$$

$$v^q = u^q_q - R^q_s i^q_q \tag{3.5}$$

v:s initial value is given by its transfer function Eq. (1.12) and the final value theorem and is dependent on R_s, R_r and u_q. As can be seen in Tbl. 3.4 the step response when $u_q = H(t)$ is applied varies marginally although R_s and R_r differs with several orders of magnitude. The problem should thereby apply for all motor sizes.

	1,5kW	30 kW	500 kW
R_s	4.017	0.086	0.00219
R_r	2.833	0.053	0.00157
$v(0)$	0.414	0.381	0.418

Table 3.4: R_s, R_r and v for several motor sizes

The SNR_{ADC} for our test equipment AD converter is approximately $72dB$.

Increasing u_q without rotation will cause the voltage vector $\vec{u}_{dq}$ and the corresponding stator voltages to grow. The lack of rotation and the increasing current flowing through the stator will cause a increasing magnetization. This corresponds well to observation 2.

To compare the different effects of rounding simulation where $R_s i_q$ was rounded and floored (always towards zero) were performed, see Fig. 3.31. Using the round function a dead-lock behavior was observed. The nonlinear behavior of the systems make direct comparisons tricky.

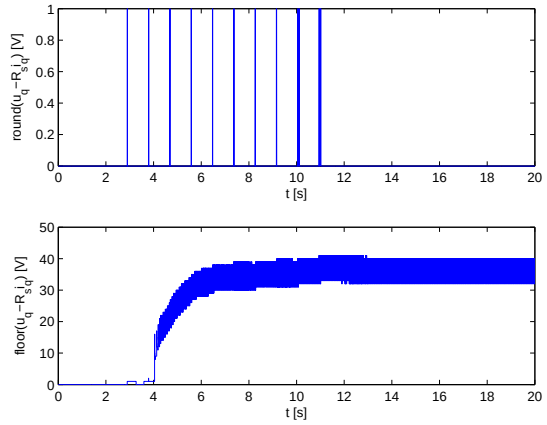

t	0	1	12
u_q	0	0	1

Figure 3.31: $v = u_q - R_s i_q$ for simulations using round and floor respectively

Chapter 4

Discussion

Our hypothesis is that one or several of condition 1-3 on page section 3.1 fail to be satisfied. This will be investigated with the observations from section 1.3 in mind. The first condition is assumed to be met since the motor is magnetized at dead-lock according to NFO.

4.1 Asynchronous AC motor

Eqs. (1.1)-(1.4) form a nonlinear differential equation system that can not be solved analytically. After transformation into the dq coordinate system the equations are still nonlinear but the angle dependent term $e^{j\epsilon}$ is eliminated. The lack of observability at zero stator frequency will cause every attempt to control the motor at this state to fail. This is the initial state for our controller and it is necessary to leave it as fast as possible.

Some small difference between the motor models can be noted in Fig. 3.1. Parts of the oscillative differences of Δm_e can be eliminated by the reducing initial value of i_{mr} in the model provided by NFO. For the remaining oscillations and the Δm_e offset no explanation has been found. Since both models are based on the same equations we assume the differences are due to numerical properties. Fig. 3.2 offers a comparison between the two models and Fig. 3.3 is a plot of the same test sequence but run on the actual motor. The biggest difference between the models and the real motor is the lack of friction in the model. This explains the (small) speed error if Fig. 3.3. One advantage of the NFO model is the direct access to ρ. By comparing the real and estimated value the regulators ability to estimate all other quantities can be measured. A subjective observations is that simulations tend to be quicker with the NFO model.

All three conditions derived for avoiding dead-lock are undoubtedly necessary. There is a possibility that more conditions as to be fulfilled to ensure rotation. For example the initial change ρ might have to exceed a certain rate to leave the unobservable state.

4.2 Variable Speed Drive

No evidence contradicting of the assumptions about the analog circuitry made in section 1.6 have been observed. Since only low frequencies has been used

this is not very surprising. The results from the modifications indicates that pre-quantization is the most efficient way of avoiding the dead-lock.

4.3 Friction

Considering the results from 3.3 the dead-lock is unlikely due to friction. To reduce the impact of the friction the following improvement may be introduced:

Improvement If m_c is known the current required to eliminate frictional torque can be calculated using Eq. (4.1). Eq. (4.2) modifies the i_q reference to compensate for friction. The idea is the same as presented in [10, eq. (10)] albeit with a less complex friction model. A simple experiment for obtaining m_c is presented in 2.3.

$$i_{q_{min}} = \frac{3}{2}\frac{m_c}{(1-\sigma)L_s i_{mr}} \tag{4.1}$$

$$i_{q_f} = sgn(i_q)i_{q_{min}} + i_q \tag{4.2}$$

If speed controller like Eq. (2.2) are used, the frictional torque will be compensated for automatically but with a small delay making this not necessary improvement.

Simulations with the estimated m_c show acceptable agreement with the experimental results for low frequencies when the Dahl model is used, Fig. 3.5. At higher speeds a frequency dependent term must probably be used. Since only low speed properties are of interest this has not been investigated further.

4.4 Parameters

The most critical parameter at low speed is R_s. As seen in Eq. (1.21) it does not only affect the magnitude of $\dot{\rho}$ but also its sign. Overestimating R_s by a few percent will cause the regulator to fail, Fig 3.11. Underestimation of R_s or erroneous estimates of the other will decrease the controllers performance but have less severe impact on stability.

Parameter sensitivity

Slow ramp (0.1 Hz/s) In Fig. 3.8 the normal behavior - derived by using the correct motor parameters in the controller - of the motor is shown. For the rest of the discussion about the slow ramp experiment this figure is the "norm". Notice that the "real" signal is somewhat distorted, even so this is considered the true value.

There is no real difference between the "norm" and Fig. 3.9. This indicates that underestimating R_s doesn't greatly impact the controller at low speeds but 3.20 demonstrate that R_s do have influence on the controller. Therefore, to set R_s low on purpose to avoid over estimation is not such a good idea.

It is interesting to see that it is a variation between running with R_s at 110% (shown in 3.10) to running with R_s at 115% (shown in Fig. 3.11). Most noticeable is the contrast in the estimation. In the bottom half of Fig. 3.11,

which describes the differnece between the "real" and the estimated signal, the estimation of the real signal is horrible. It seems that running the controller with just a slightly, a couple of per cents, too big value on R_s will cause the controller to be unstable.

Running with L_s at only 35% of the true value, seen in Fig. 3.13, gives good results and behavior. Only after stepping down further (Fig. 3.12), somewhat poor behavior is noted. Even so the controller reaches it correct value and running with R_s at 30% is probably not a problem.

In the bottom half of Fig. 3.15 the estimation is very far from the real value. Quantisation is the probable reason for that all the "spikes" have equal amplitude. This phenomena is also seen in Fig. 3.11. The upper bound for L_s is around 125 % and can the corresponing plot can be seen in Fig. 3.14.

By comparing Fig. 3.16 and Fig. 3.17 with the "norm" it is clear that R_R doesn't have any impact on the controller if controlling without any load. The sensitivity of R_R is probably much more noticeable if there would have been a load connected to the motor. This is something that is not tested in this thesis.

Mixed test sequence It is no surprise that R_S greatly impacts the behavior of the mixed test sequence. What is worth noticing is that a lower bound of R_S is found - seen in Fig. 3.21 - something that was not found in the slow ramp test. Using R_S at 50 % doesn't provide a perfect controller but it follows the reference signal well.

Quite amazingly, the controller manage to follow the reference signal even though there is a 30 % overestimation error in R_S (seen in Fig. 3.22. This should be compared to the slow ramp experiment where an error of 15% caused the controller to loose the ability to estimate the real value correctly. This should mean that a slow ramp is harder to control than a faster (mixed) signal. In Fig. 3.23 once again the same size "spikes" are observed.

In the tests that were run no lower limit was found for L_S. In Fig. 3.24 the controller still manage to follow the reference. Judging from the slow ramp experiment when using small values of L_S (seen in Fig. 3.12 and 3.13), somewhere in this region the lower limit would be found if more experiments were conducted.

In Fig. 3.26, oscillations are noticed after 9 sec. Since the test sequence ended premature, these oscillations grew strong enough to trigger the built-in safety switch. It is worth noticing the radical change in behavior, just going from L_S at 110 % and 120 %. Since no oscillations, what so ever, was seen in Fig. 3.25 (representing L_S at 110 %). These types of oscillations are also seen in Fig. 3.29. Also there the built-in safety switch get triggered (after 11 seconds).

No lower limit was found for σ. This corresponds well to the findings for the slow ramp experiment (Fig. 3.18), also in that experiment no lower limit was found for σ. Opposite to the situation with R_S, where no lower bound was found in the slow ramp experiment but one was found in the mixed test sequence experiment, no conclusion can be drawn about the lower bound of σ.

Fig. 3.28 is actually the "norm" for the experiment. Surprisingly it is also represents the upper bound for σ. As mention above, oscillations can be seen in Fig. 3.29 (the figure that represents σ at 110 %). That indicates that using σ at that level (110 %), is not recommended.

4.5 Measurements

The noise covariance is close to zero indicating white noise [11]. This is strengthen by the FFT plotted in Fig. 3.5. A small deviation from the constant white noise's spectrum can be seen at low frequencies. The noise measurements indicates that the noise SNR is very good even for small motors.

4.6 Quantization

[13] concludes that analyzing the whole system analytically is difficult. Our analysis has targeted the weakest part of the implementation, the smallest signal at startup.

With the help of Eq. (1.29) and the actual values of the reference system the smallest representable difference of Eq. (3.5) is calculated to $0.1[V]$. At low speeds this is far lower than $0.1[V]$ implying Eq. (3.4) should never be fulfilled. Without a change in ρ the magnetic field will not rotate and v will not increase. The system is dead-locked.

The salvation is the motors time constants. A step change in applied voltage will not result in a current step, Fig 3.4. For a short period of time v will increase well beyond the required $0.1[V]$ given the step applied is big enough. Due to the quantization of the system changes in control signal will always occur as steps.

Improvement To avoid dead lock steps at least $10x_{d_{min}}$ is preferable. This can be achieved by pre-quantizing u_q:

$$u_{q_{pre-quant}} = u_q - mod(u_q, 10u_{q_{min}})$$

Decreasing T_s for the speed loop (Eq. (2.2)) will have a similar effect as indicated in Eq. (1.10). Note that this modification is only necessary at low speeds ($\omega < 2[Hz]$).

The results in Tbl. 3.2 show that pre-quantization is the most effective way of dealing with the problem.

$e_q(t)$ might induce systematic errors into the open integration of Eq. (1.20). This error may be used to our advantage. By using the floor function on $R_s i_q$ in Eq. (3.5) condition (3.4) will be fulfilled as soon as $u_q \neq 0$. Fig. 3.31 illustrates the different results retrieved when using different rounding methods. When using the round function the system dead-locks while using the floor function works well. The delay noticed while using the floor function equals the time it takes before the first change in ρ.

This measured SNR_{ADC} is close to the SNR for the whole current measurement system indicating that the controller would not profit from more accurate current transducers.

Observation 4 may be explained by the implementation of the fraction in Eq. (3.4). High power motors have larger magnetizing currents and hence the fraction will decrease in size.

Improvement Eq. (4.3) suggest a improvement to ease these troubles. By multiplying the sum instead of each individual term the roundoff problems should be avoided.

$$\dot{\rho} = \sum_{0}^{t} \lfloor \frac{T_s}{L_s^q i_{mr}^q} v^q \rfloor \approx \lfloor \frac{T_s}{L_s^q i_{mr}^q} \rfloor \sum_{0}^{t} \lfloor v^q \rfloor \tag{4.3}$$

Chapter 5

Conclusion

For 120 years the asynchronous motor has protected its secrets well. By using field orientation its mysteries are fading away and reasonable performing controllers have emerged. Perfect control is and will be an utopia due to the lack of observability at certain states.

The performance of the NFO algorithm is so far limited by digital implementation. In simulation no dead-lock has been observed as long as the model parameters are kept reasonably close to the actual values. If quantization is introduced into simulation dead-lock may occur even with a perfect match between the motor parameters and the parameters used in the controller.

Several solutions have been proposed and implemented with different levels of success. The pre-quantization seems to be the most trustworthy way to go. A proper implementation has to be tested at NFO to confirm this.

5.1 Future work

- If there exist more conditions than the three found this might be interesting for future optimization and performance calculations on the controller.
- Implementing the regulator into a floating point DSP should produce the same results as seen in the simulations. In this way the lower limit for controlling the motor should further be reduced.
- To ensure the proper start of the motor some theory for leaving the unobservable state should be developed. Our proposal to increase the quantization level is one way of doing this but this is not proven analytically.

Bibliography

[1] R. Jönsson, (1992), *Method and apparatus for controlling an AC induction motor by indirect measurement of the air-gap voltage*, US patent no 5294876

[2] R. Jönsson, (1989), *Method and means for controlling a bridge circuit* , US patent no 4947309

[3] Lidow, A., (2003) *The Power Conversion Process as a Prosperity Machine Part II - Power Semiconductor Road Map*, APEC 2003.

[4] M.L. Aime, M.W. Degner, R.D. Lorenz, (1998), *Saturation Measurements in AC Machines Using Carrier Signal Injection* The 1998 IEEE Volume 1, 12-15 Oct. Page(s):159-166

[5] W. Leonhard, (2001), *Control of Electrical drives*, Springer Verlag Berlin

[6] P. Dahl, (1968), *A solid friction model*, Technical Report TOR-0158(3107-18)-1, The Aerospace Corporation, El Segundo, CA

[7] C Canudas de Wit, K. J. Åström and P Lischinsky, (1995), *A new model for control of systems with friction*, IEEE Transactions on Automatic Control Volume 40, Issue 3, March 1995 Page(s):419-425

[8] P Vaclavek, P Blaha, (2006), *AC Induction Machine Observability Analysis and its Impact on Sensorless Control Algorithms*, International Conference on Intelligent Engineering Systems, INES '06, Proceedings, 26-28 Jun. Page(s):63-68

[9] H.Olsson, K.J Åström, C.Canudas de Wit, M Gäfvert, P.Lischinsky, (1998), *Friction Models and Friction Compensation*, European Journal of Control

[10] A. Robertsson, A. Shiriaev, R. Johansson, (2003), *Friction compensation for nonlinear systems based on the LuGre model*, Proc. 2nd IFAC Workshop on Lagrangian and Hamiltonian Methods for Nonlinear Control. Pages 183-188

[11] F Gustavsson, L Ljung, M Millnert, (2001), *Digital Signalbehandlig*, Studentlitteratud Lund

[12] S Wade, M W Dunnigan, B W Williams, 1994, *Paramter identification for vector controlled induction machines*, International Conference on Control, Control '94. Volume 2, Page(s):1187-1192

[13] M Konghirun, L Xu, J Skinner-Gray, 2004, *Quantization errors in digital motor control systems*, The 4th International Power Electronics and Motion Control Conference, IPEMC 2004, Page(s):1421-1426

[14] Peter Vas, (1993), *Parameter Estimation, Condition Monitoring, and Diagnosis of Electrical Machines*, Clarendon Press Oxford

[15] NFO Drives AB, (2006), *Användar och installationshandbok NFO Sinus 1,5-15kW 400V*, Version 3.1

[16] Joachim Holtz, (2002), *Sensorless Control of Induction Motor Drives*, Proceedings of the IEEE, Volume 90, Issue 8, Page(s):1359 - 1394

[17] http://focus.ti.com/docs/prod/folders/print/tms320f2806.html

[18] J.D. Glover, M. Sarma, (1994), *Power system analysis and design*, PWS Publishing Company, Boston

[19] http://www.mathworks.com/access/helpdesk/help/toolbox/physmod/powersys/ref/asynchronousmachine.html

[20] http://en.wikipedia.org/wiki/Quantization_noise

Appendix A

The Three-phase System; Vector, ab and dq Representation

Three-phase electric power systems have at least three conductors carrying sinusodial voltage waveforms 120° offseted in time. In the complex plane, this may be represented with three voltage vectors with varying amplitude but constant angle between them, Fig A.1. Using the trigonometric functions transformation from the vector notation to a orthogonal reference system is possible. The result is Eq. A.2 where the second equality is possible due to Eq. A.1.

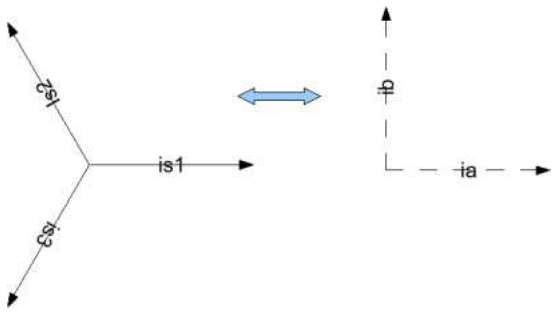

Figure A.1: Vector and ab-representation

$$i_r + i_s + i_t = 0 \tag{A.1}$$

$$\begin{pmatrix} i_a \\ i_b \end{pmatrix} = \begin{pmatrix} 1 & -\frac{1}{2} & -\frac{1}{2} \\ 0 & \frac{\sqrt{3}}{2} & -\frac{\sqrt{3}}{2} \end{pmatrix} \begin{pmatrix} i_r \\ i_s \\ i_t \end{pmatrix} = \frac{\sqrt{3}}{2} \cdot \begin{pmatrix} \sqrt{3} & 0 & 0 \\ 0 & 1 & -1 \end{pmatrix} \begin{pmatrix} i_r \\ i_s \\ i_t \end{pmatrix} \tag{A.2}$$

The next step is to transform i_a and i_b into field orientation currents i_d and i_q. This is done by a rotation with the angle ρ as in Fig A.2.

$$\begin{pmatrix} i_d \\ i_q \end{pmatrix} = \begin{pmatrix} \cos(\rho) & \sin(\rho) \\ -\sin(\rho) & \cos(\rho) \end{pmatrix} \begin{pmatrix} i_a \\ i_b \end{pmatrix} \tag{A.3}$$

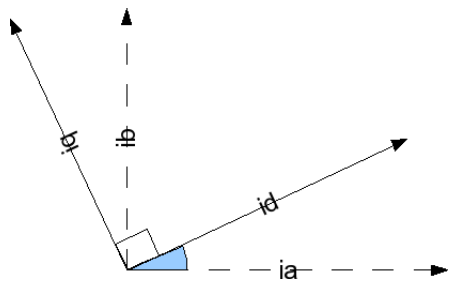

Figure A.2: Rotation of ab coordinate system

Appendix B

Reference equipment data

Measured parameters are acquired according to protocols specified in 2.4. * marked parameters are estimated or retrieved from [15].

Motor	ABB (Green)	ASEA (blue)
$P_0[W]$*	1500	1500
$Us_0[V]$	400	400
$R_s[\Omega]$	4.8	4.4
$R_r[\Omega]$*	3	2.92
$L_s[H]$*	0.382	0.382
$cos(\phi)$	0.79	0.79
$\|i_{mr}\|[A]$*	1.84	1.84
$i_{max}[A]$	4.20	4.20
$poles$	4	4

Table B.1: Motor paramaters, ABB motors parameters used in simulation

Signal	Wire color
Phase R	Red
Phase S	Green
Phase T	Yellow
Power enable	Blue
Power ground	Black

Table B.2: Control card wireing

Measurement point	Phase R	Phase S	Phase T
Simulink	10	10	
Analog out	9.9943	9.9945	
After ISO124	9.8717	9.8513	
Out	0.1297	0.1314	Saturated
Simulink	-10	-10	
Analog out	-9.9962	-9.996	
After ISO124	-10.0158	-9.9846	
Out	4.8093	4.8160	Saturated
Simulink	0	0	
Analog out	-0.0039	-0.0035	
After ISO124	-0.0032	0.0047	
Out	2.5148	2.5110	No measurement
Simulink	8	8	
Analog out	7.9925	7.9926	
After ISO124	8.0059	7.9947	
Out	0.5136	0.5142	Saturated
Simulink	4	4	
Analog out			
After ISO124			
Out	1.5157	1.5177	4.5148
Simulink	-4	-4	
Analog out			
After ISO124			
Out	3.5168	3.5147	0.5170
Simulink	0	0	
Analog out			
After ISO124			
Out	2.5162	2.5162	2.5162

Table B.3: Gain verification measurements

	Lab equipment	NFO-Sinus
D/A	12-bit	12-bit
A/D	12-bit	10-bit
T_s	1/1000	1/7000
Phase T	Analog calculation	Digital calculation
Current measurement	+- 1%	+-1%
Vector rotators	Double representation	Lookup table
Dead-time compensation for PWM	No	Yes
Feedback D/A	No	Yes
Control unit	PC	DSP
Signal representation	Double, d_{nn}	d_{12}
Real-time controller	No	Yes
Current measurement units	LEM 300A	LEM 10A

Table B.4: Equipment differences

Start sequence To charge the bootstrap capacitors and make sure all the power transistors are operative the bootstrap sequence described by Fig. B is used. The sequence is applied simultaneously on all three phases every time a new simulation starts. A disturbance of the rotor position is observed due to this. Due to lack of control over phase t the bootstrap sequence is applied with reversed polarity.

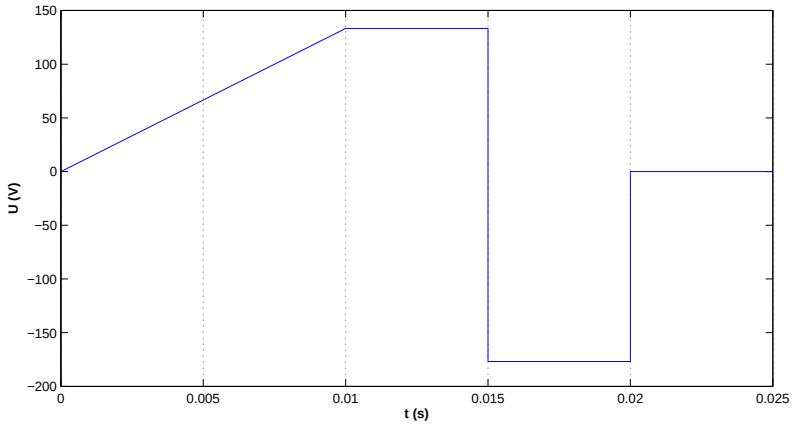

t [ms]	0	10	15	15	20	20
Applied voltage [V]	0	$\frac{1}{3}U_{max}$	$\frac{1}{3}U_{max}$	$-\frac{1}{2}U_{max}$	$-\frac{1}{2}U_{max}$	0

Figure B.1: Bootstrap sequence

Appendix C

Matlab code

C.1 m_c calculation

```
%Calculate m_c and plot measured and simulated data

timespan=5; %Plot time length
t=0:h:timespan; %x-axis to plot
%load friction_data.mat;
s_s=[13145 8963 8872]; %Power unplug sample - 0.2s/h
friction_m=zeros(timespan/h+1,3); %Size of friction measurement matrix
friction_m(:,1)=f_2hz.signals.values(s_s(1):s_s(1)+timespan/h,1);
friction_m(:,2)=f_5hz.signals.values(s_s(2):s_s(2)+timespan/h,1);
friction_m(:,3)=f_10hz.signals.values(s_s(3):s_s(3)+timespan/h,1);
friction_m=friction_m-0.03; %Remove offset
[B,A]=butter(1,0.1); %Butterworth filter for removing sampling noise.
friction_m=filtfilt(B,A,friction_m); %Filter measurements

s_s=[9800 9800 9800]; %"Power unplug" in simulation -0.2s/h
friction_s=zeros(timespan/h+1,3); %Size of friction simulation matrix
friction_s(:,1)=f_sim_2_hz.values(s_s(1):s_s(1)+timespan/h,2);
friction_s(:,2)=f_sim_5_hz.values(s_s(2):s_s(2)+timespan/h,2);
friction_s(:,3)=f_sim_10_hz.values(s_s(3):s_s(3)+timespan/h,2);


k=zeros(1,3);
for i=1:5000    %Find stopstime for rotor
    if(k(1)==0 && friction_m(i,1) < 0.025)
        k(1)=i;
    end
    if(k(2)==0 && friction_m(i,2) < 0.025)
        k(2)=i;
    end
    if(k(3)==0 && friction_m(i,3) < 0.025)
        k(3)=i;
    end
```

```
end
k=(k-300) %Remove impact of brakeing electromagnetic torque
k=k./friction_m(1,:)*h %calculate dw/dt,

%Plot measured data and simulation
figure(1);
plot(t,friction_m,'b',t,friction_s,'r--');
xlabel('t [s]')
ylabel('f [Hz]')
legend('Measurements 2,5,10 [Hz]');
```

C.2 Filter measured signals

```
%Create butterworthfilter and filter signal
function y=filter_sig(x)
[B,A]=butter(1,0.04);
y=filtfilt(B,A,x);
```

Appendix D

Parameters

D.1 Matlab code

```
function ps_test_script(param)
% FILES AND PATHS
FILE_MODEL_INIT = { 'init_system_h_2';
                    'calculate_constants_discrete_controller'
            };
FILE_SIM_MODEL  = 'ps_testbench';
FIG_FILENAME    = 'ps';

% SIMULATION PARAMS
START_TIME  = 0;
END_TIME    = 15;

%%%%%%%%%%%%%%%%%%%%%%%%%%%%%%%%%%%%%%%%%%%%%%%%%%%%%%%%%%%%%%%%%%%%%%%
% PARAMS
%%%%%%%%%%%%%%%%%%%%%%%%%%%%%%%%%%%%%%%%%%%%%%%%%%%%%%%%%%%%%%%%%%%%%%%

% DEFAULT
RS_RANGE    = 1.0;
LS_RANGE    = 1.0;
RR_RANGE    = 1.0;
SG_RANGE    = 1.0;
%RANGE      = 0.8:0.05:1.2;
RANGE       = 0.3:0.05:1.5;


% DYNAMIC
if (param == 'rs')
    RS_RANGE = RANGE;
end
if (param == 'ls')
    LS_RANGE = RANGE;
end
```

```
if (param == 'rr')
    RR_RANGE = RANGE;
end
if (param == 'sg')
    SG_RANGE = RANGE;
end
%%%%%%%%%%%%%%%%%%%%%%%%%%%%%%%%%%%%%%%%%%%%%%%%%%%%%%%%%%%%%%%%%%%%%%%


%%%%%%%%%%%%%%%%%%%%%%%%%%%%%%%%%%%%%%%%%%%%%%%%%%%%%%%%%%%%%%%%%%%%%%%
 % LINE CHARACTERISTICS IN PLOT
LINE_ONE  = ['k' '-'];  % Black and solid
LINE_TWO  = ['r' '-.']; % Red and dashed-dot
X_LABEL = 'time / s';
Y_LABEL = 'amp / V';

TITLE_ONE = 'REFERENCE vs. REAL';
TITLE_TWO = 'REAL vs. ESTIMATION';
%%%%%%%%%%%%%%%%%%%%%%%%%%%%%%%%%%%%%%%%%%%%%%%%%%%%%%%%%%%%%%%%%%%%%%%


%%%%%%%%%%%%%%%%%%%%%%%%%%%%%%%%%%%%%%%%%%%%%%%%%%%%%%%%%%%%%%%%%%%%%%%
for iii=1:size(FILE_MODEL_INIT,1)
    run (char(FILE_MODEL_INIT(iii)));
end

OPTIONS = simget(FILE_SIM_MODEL); % GET CURRENT
OPTIONS = simset(OPTIONS, 'SrcWorkspace', 'current');
%%%%%%%%%%%%%%%%%%%%%%%%%%%%%%%%%%%%%%%%%%%%%%%%%%%%%%%%%%%%%%%%%%%%%%%


%%%%%%%%%%%%%%%%%%%%%%%%%%%%%%%%%%%%%%%%%%%%%%%%%%%%%%%%%%%%%%%%%%%%%%%
rs_cnt = 0;
for Rs_disc_model=RS_RANGE*Rs_disc_model
 rs_cnt = rs_cnt + 1;

 ls_cnt = 0;
 for Ls_disc_model=LS_RANGE*Ls_disc_model
  ls_cnt = ls_cnt + 1;

  rr_cnt = 0;
  for Rr_model=RR_RANGE*Rr_model
   rr_cnt = rr_cnt + 1;

   sg_cnt = 0;
   for Sigma_disc_model=SG_RANGE*Sigma_disc_model
     sg_cnt = sg_cnt + 1;

      % RUN SIMULINK MODEL
      sim(FILE_SIM_MODEL, [START_TIME END_TIME], ...
```

```
    OPTIONS);

% COLLECT DATA FROM SIMULINK
time = TIME;
ref  = REF;
real = REAL;
nfo  = NFO;

% MAKE THEM OF EQUAL LENGTH
SIZE    = size(time,1);
SIZE(2) = size(ref,1);
SIZE(3) = size(real,1);
SIZE(4) = size(NFO,1);
length  = min(SIZE);
time    = time(1:length);
ref     = ref(1:length);
real    = real(1:length);
nfo     = nfo(1:length);

% PLOT
fig_id = figure;

% 1) REFERENCE vs. REAL
TITLE = ...
  sprintf('%s\n Rs:%0.3g%% Ls:%0.3g%% ...
  Rr:%0.3g%% Sg:%0.3g%%', ...
  TITLE_ONE, 100*RS_RANGE(rs_cnt),...
  100*LS_RANGE(ls_cnt), ...
  100*RR_RANGE(rr_cnt), 100*SG_RANGE(sg_cnt));

 subplot(2,1,1); grid on; hold on;
 plot(time, ref  , LINE_ONE);
 plot(time, real , LINE_TWO);
 legend('REF', 'REAL', 'Location','EastOutside');
 xlabel(X_LABEL); ylabel(Y_LABEL); title(TITLE);

 % 2) REFERENCE vs. NFO
 TITLE = ...
  sprintf('%s\n Rs:%0.3g%% Ls:%0.3g%%
  Rr:%0.3g%% Sg:%0.3g%%', ...
  TITLE_TWO, 100*RS_RANGE(rs_cnt),...
  100*LS_RANGE(ls_cnt), ...
  100*RR_RANGE(rr_cnt), 100*SG_RANGE(sg_cnt));

 subplot(2,1,2); grid on; hold on;
 plot(time, real , LINE_ONE);
 plot(time, nfo  , LINE_TWO);
 legend('REAL', 'EST', 'Location','EastOutside');
 xlabel(X_LABEL); ylabel(Y_LABEL); title(TITLE);
```

```
        % THE FILENAME OF THE .JPG
        fig_filename = ...
         sprintf('30NOV/%s__Rs_%0.3g_Ls_%0.3...
         g_Rr_%0.3g_Sg_%0.3g__%s.jpg', ...
         FILE_SIM_MODEL, RS_RANGE(rs_cnt),...
         LS_RANGE(ls_cnt), ...
         RR_RANGE(rr_cnt),SG_RANGE(sg_cnt), ...
         datestr(clock,30));

        % SAVE THE FIGURE
        saveas(fig_id, fig_filename, 'jpg');
        close;
       end
  end
 end
end
%%%%%%%%%%%%%%%%%%%%%%%%%%%%%%%%%%%%%%%%%%%%%%%%%%%%%%%%%%%%%%%%%%%%%%%%%%%%%%%
```

D.2 Simulink scheme

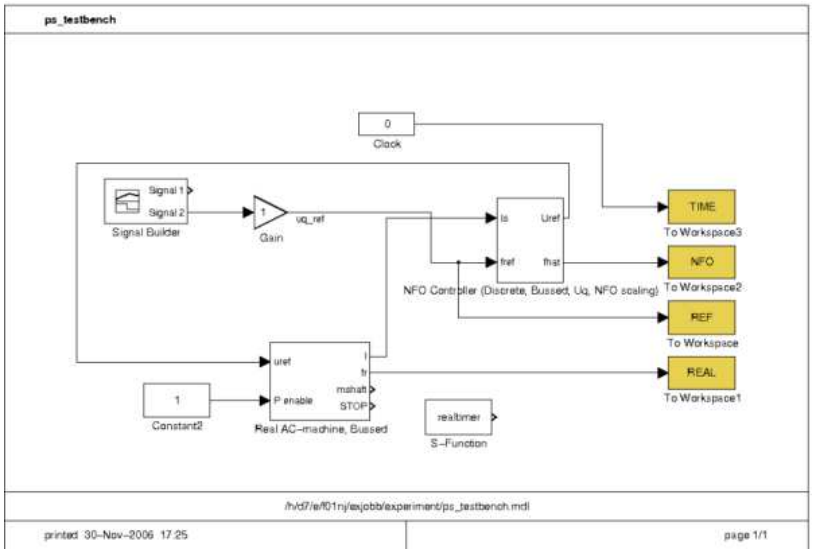

Figure D.1: Simulink scheme

D.3 Parameter estimation

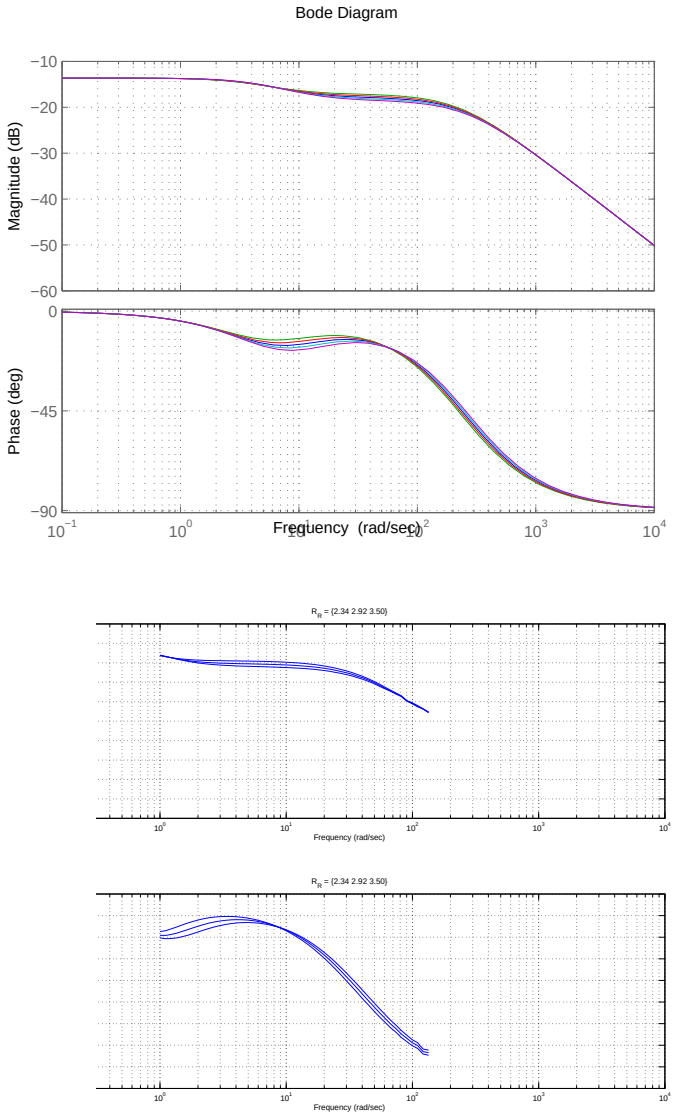

Figure D.2: Bode plot and simulation results for different values of R_r

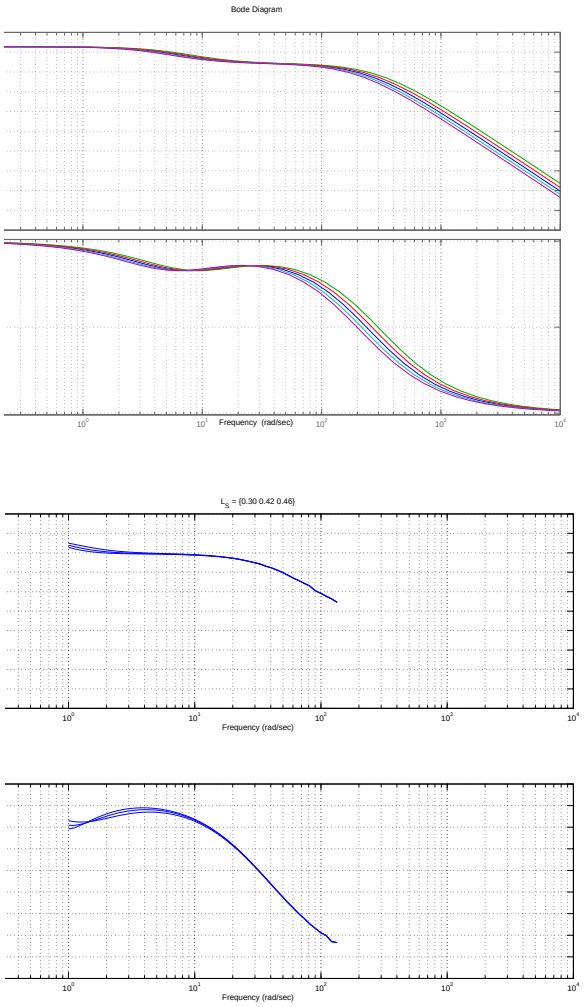

Figure D.3: Bode plot and simulation results for different values of L_s

Appendix E

Schematics and board layout

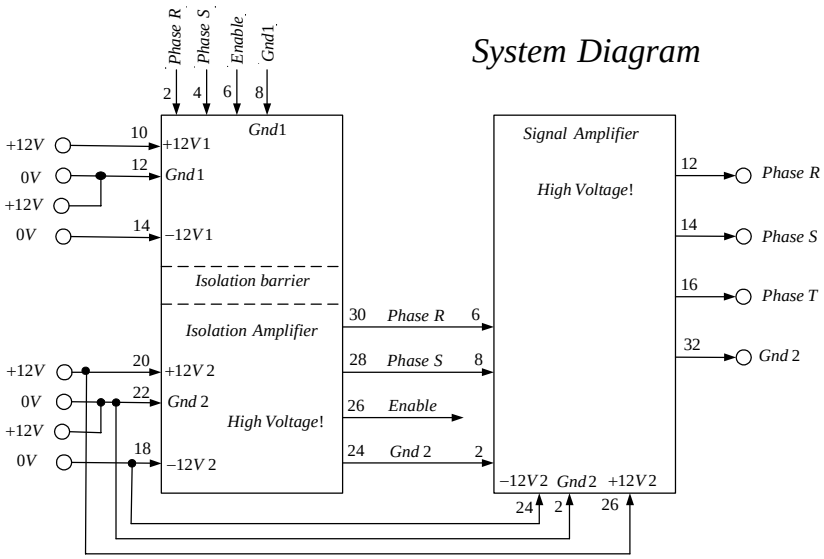

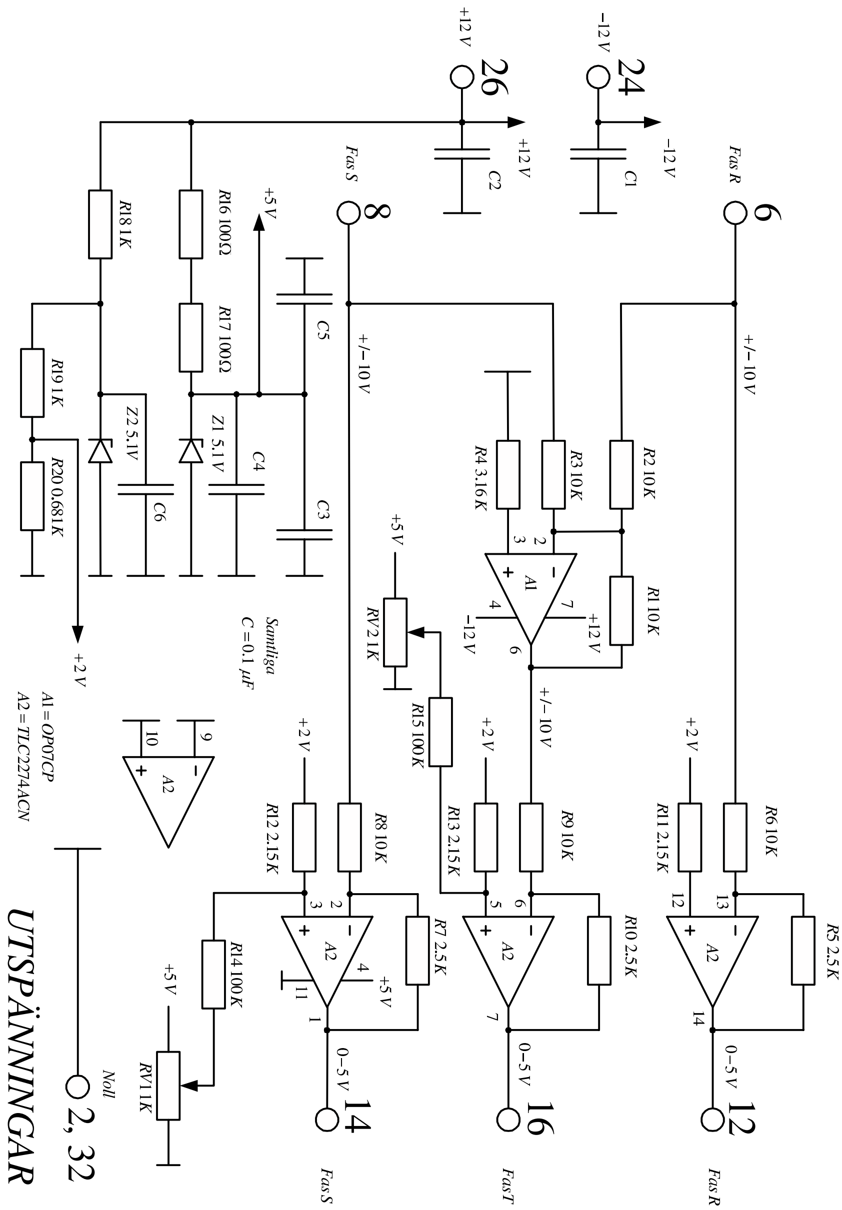
UTSPÄNNINGAR
26
+12 V
24
−12 V
+12V
−12V
C1
C2
Fas S
8
Fas R
6
+/− 10V
+/− 10V
R18 1K
R16 100Ω
R17 100Ω
+5V
C5
C4
C3
C6
R19 1K
R20 0.681K
Z2 5.1V
Z1 5.1V
+2 V
Samtliga
C = 0.1 µF
A1 = OP07CP
A2 = TLC2274ACN
R4 3.16K
R3 10K
R2 10K
R1 10K
A1
−12V
+12V
+/− 10V
RV2 1K
R15 100K
R8 10K
R12 2.15K
R13 2.15K
R9 10K
R11 2.15K
R6 10K
R7 2.5K
R10 2.5K
R5 2.5K
A2
R14 100K
RV1 1K
Noll
2, 32
0−5 V
14
16
12
Fas S
Fas T
Fas R

Appendix F

Dahl-friction model for rotating bodies

The Dahl friction model as stated in [6]:

$$\frac{dF}{dt} = \sigma \left(1 - \frac{F}{F_c} sgn(v)\right) v \tag{F.1}$$

The relationship between force (F) and torque (m) from mechanics

$$m = Fl \tag{F.2}$$

The angular veliocity from a circle with the radius r and boundaryspeed v:

$$\omega = vr \tag{F.3}$$

Eqs. F.1, F.2 and F.3 gives:

$$\frac{dm}{dt} = \sigma r \left(1 - \frac{m}{m_c} sgn(\omega)\right) \omega \tag{F.4}$$

where r is approximated with 1 since $\sigma \gg r$.